TÜBİTAK

Turkish Journal of Chemistry

http://journals.tubitak.gov.tr/chem/

Research Article

Turk J Chem
(2020) 44: 1395-1409
© TÜBİTAK
doi:10.3906/kim-2006-22

Synthesis, characterization and evaluation of antidengue activity of enantiomeric Schiff bases derived from S-substituted dithiocarbazate

Maqsood MARYAM[1,2], Sang Loon TAN[3], Karen Ann CROUSE[3], Mohamed Ibrahim MOHAMED TAHIR[3], Hui-Yee CHEE[2,*]

[1]Faculty of Natural Sciences, Sardar Bahadur Khan Women University, Balochistan, Quetta, Pakistan
[2]Department of Medical Microbiology and Parasitology, Faculty of Medicine and Health Sciences, Universiti Putra Malaysia, SerdangSelangor, Malaysia
[3]Department of Chemistry, Faculty of Science, Universiti Putra Malaysia, Serdang, Selangor, Malaysia
[4]Research Centre for Crystalline Materials, School of Science and Technology, Sunway University, Sunway, Selangor, Malaysia

Received: 13.06.2020 • **Accepted/Published Online:** 05.08.2020 • **Final Version:** 26.10.2020

Abstract: A series of Schiff bases have been successfully synthesized through the acid-catalyzed condensation of S-substituted dithiocarbazates and three enantiomerically pure monoterpenes, (1*R*)-(+)-camphor, (1*S*)-(-)-camphor, (1*R*)-(-)-camphorquinone, (1*S*)-(+)-camphorquinone, (*R*)-(-)-carvone and (*S*)-(+)-carvone. Spectroscopic results revealed that the Schiff bases containing camphor or carvone likely adopted an *E*-configuration along the characteristic imine bond while those containing camphorquinone assumed a *Z*-configuration. The antidengue potential of these compounds was evaluated based on DENV 2 caused cytopathic effect (CPE) reduction-based in vitro evaluation. The compounds were validated through secondary foci forming unit reduction assay (FFURA). Compounds were also tested for their cytotoxicity against Vero cells. The compounds showed variable degrees of antiviral activity with the camphor compounds displaying the highest antidengue potential. The enantiomers of the compounds behaved almost similarly during the antiviral evaluation.

Key words: Dithiocarbazate Schiff base, enantiomers, camphor, camphorquinone, carvone, antidengue

1. Introduction

Dengue virus (DENV) is a positive single-stranded RNA virus of the Flaviviridae family that causes dengue fever (DF) with or without warning signs, and severe dengue [1]. The four serotypes, DENV 1, DENV 2, DENV 3, and DENV 4, are genetically and antigenically distinct, and epidemiologically similar [2]. Infection with one serotype leads to all-time protection against homologous reinfection but only brief protection against heterologous types. DENV infection and immune system interactions may result in either immunopathology leading to severe forms of the disease, or recovery from infection [3]. DENV is one of the most serious arboviral threats in tropical and subtropical regions, with 50–100 million new cases annually among the 4 billion people in endemic regions [4]. It is spreading rapidly due to global demographic changes, rapid and unrestrained urbanization, population growth, and global ease of travel. WHO estimates that dengue has shown a 30-fold increase in detected cases globally over the past 5 decades [1]. There is no antiviral medication currently available for the treatment of dengue.

S-substituted dithiocarbazates and their Schiff base derivatives have received increasing attention over the years in the field of medicinal chemistry owing to their versatile functionalities to act as antimicrobial [5], anticancer [6], anthelmintic [7], antioxidative [8], anti-inflammatory [9], anticonvulsant, and antinociceptive agents [10], as well as nuclear medicines [11]. While the specific mode of action remains unclear, they are commonly believed to target metal containing active sites owing to the presence of hard and soft, nitrogen and sulfur donor atoms that can form stable chelating complexes and disrupt the physiological function of the target. Such a mechanism has been demonstrated by a closely related thiosemicarbazone Schiff base analog known as triapine, which was shown to be effective against different types of cancers and viruses in several clinical trials [12]. Dithiocarbazate Schiff base derivatives warrant further exploration since a wide variety of analogs can be derived by introducing different substituents into the structural framework potentially enriching their physico-chemical and biological activities.

* Correspondence: cheehy@upm.edu.my

There are no reports on evaluation of antidengue activity of dithiocarbazate derivatives. Research in the field has mainly focused on chemical extracts from medicinal plants and herbs due to their relatively low toxicity [13]. Among the vast number of natural products, terpenes and terpenoids represent a very important class of compounds due to their wide spectrum of biological activities including antimicrobial [14], anticancer [15], and antioxidant [16] characteristics. Recently, a few monoterpenes and terpenoids have been evaluated for the first time against dengue virus. They were found to be moderately active in inhibiting the replication of all four dengue serotypes in Vero Cells [17]. In view of the medicinal benefits of these compounds, we have embarked on the synthesis of a series of Schiff bases derived from S-methyl, S-benzyldithiocarbazates, and enantiomerically pure monoterpenes comprising (1*R*)-(+)-camphor, (1*S*)-(-)-camphor, (1*R*)-(-)-camphorquinone, (1*S*)-(+)-camphorquinone, (*R*)-(-)-carvone, and (*S*)-(+)-carvone (Scheme 1) to investigate whether such combinations would be active against dengue virus while demonstrating low toxicity towards the host cells.

2. Experimental

2.1. Materials and instrumentation

Unless otherwise mentioned, all chemical reagents were of ACS grade and were used as supplied without further purification. Melting points (m.p.) were measured without correction using a Barnstead-Electrothermal IA9100 digital melting point apparatus. IR spectra were recorded on a Perkin-Elmer FT-IR 100 system using attenuated total reflection (ATR) within the spectral range 4000–250 cm^{-1}. Electronic spectra of 1×10^{-4} M solutions in DMSO were measured on a Shimadzu UV-2501PC spectrophotometer (250–800 nm). ^{1}H and $^{13}C\{^{1}H\}$ NMR spectra were recorded on a JEOL JNM-ECA 400 NMR spectrometer (^{1}H 400 MHz, ^{13}C 100 MHz) with tetramethylsilane (TMS) being used as the internal standard and DMSO-d_6 as the solvent. Mass spectra were obtained using a Shimadzu GCMS-QP5050A quadrupole mass spectrometer in electron ionization (EI) mode with direct insertion (DI). Carbon, hydrogen, and nitrogen analyses were performed on a LECO CHNS-932 analyzer under helium atmosphere with sulfamethazine being used as the standard. S-methyl (SMDTC) and S-benzyldithiocarbazates (SBDTC) were synthesized following reported procedures [18]. SMDTC (m.p. 354 K, 4.40 g, yield 72%); SBDTC (m.p. 398 K, 7.44 g, yield 75%).

2.2. Crystal structure determination

Diffraction data were collected at 150 K using an Enraf-Nonius Kappa CCD diffractometer with graphite-monochromatized Mo *K*α radiation (λ = 0.71073 Å). A multi-scan absorption correction was applied through DENZO-SMN package [19]. The structures were solved by dual-space algorithm and refined on *F*2 by full matrix least-squares technique [20]with the anisotropic displacement parameters for all nonhydrogen atoms, of which the entire process was achieved through OLEX2 program [21]. The C-bound H atoms were placed at ideal geometrical position and refined in the riding model approximation with $U_{iso}(H) = 1.2–1.5U_{eq}$ (carrier atom). The N-bound H atoms were located from difference maps and refined with $U_{iso}(H) = 1.2U_{eq}(N)$. The absolute structure was determined based on differences in Friedel pairs included

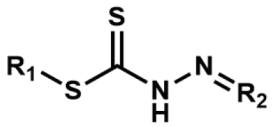

1. SMRCM; $R_1 = CH_3$, R_2 = (1*R*)-(+)-camphor
2. SMSCM; $R_1 = CH_3$, R_2 = (1*S*)-(-)-camphor
3. SMRCQ; $R_1 = CH_3$, R_2 = (1*R*)-(-)-camphorquinone
4. SMSCQ; $R_1 = CH_3$, R_2 = (1*S*)-(+)-camphorquinone
5. SMRCV; $R_1 = CH_3$, R_2 = (*R*)-(-)-carvone
6. SMSCV; $R_1 = CH_3$, R_2 = (*S*)-(+)-carvone
7. SBRCM; $R_1 = CH_2C_6H_5$, R_2 = (1*R*)-(+)-camphor
8. SBSCM; $R_1 = CH_2C_6H_5$, R_2 = (1*S*)-(-)-camphor
9. SBRCQ; $R_1 = CH_2C_6H_5$, R_2 = (1*R*)-(-)-camphorquinone
10. SBSCQ; $R_1 = CH_2C_6H_5$, R_2 = (1*S*)-(+)-camphorquinone
11. SBRCV; $R_1 = CH_2C_6H_5$, R_2 = (*R*)-(-)-carvone
12. SBSCV; $R_1 = CH_2C_6H_5$, R_2 = (*S*)-(+)-carvone

Scheme 1. Synthesis of S-substituted dithiocarbazate Schiff bases.

in the data set. The molecular structures and their packing diagrams were generated using ORTEP [22], and DIAMOND [23] respectively while the crystal data were analyzed by PLATON [24]. Details of unit cell data, X-ray data collection, and structure refinement are given in Table 1.

2.3. General procedure for the preparation of compounds 1–4 and 7–10

An equimolar amount of enantiomeric pure (1*R*)-(+)-camphor (98%, Sigma-Aldrich Chemie GmbH, Steinheim, Germany; 1.52 g), (1*S*)-(-)-camphor (99%, Sigma-Aldrich Chemie GmbH; 1.52 g), (1*R*)-(-)-camphorquinone (99%, Sigma-Aldrich Chemie GmbH; 1.66 g), or (1*S*)-(+)-camphorquinone (99%, Sigma-Aldrich Chemie GmbH; 1.66 g) was added to 0.01 mol, 1.22 g of SMDTC (or 0.01 mol, 1.98 g of SBDTC) dissolved in hot methanol (30 mL). Concentrated hydrochloric acid (37%, Merck KGaA, Darmstadt, Germany; 1.5 mL) was then added. The solution was reduced to half the initial volume and further heated for half an hour before being left to cool at ambient temperature. The product was filtered, washed with cold methanol, and recrystallized from methanol.

2.3.1. Methyl (E)-2-((1R,4R)-1,7,7-trimethylbicyclo[2.2.1]heptan-2-ylidene)hydrazine-1-carbodithioate, SMRCM (**1**). White powder; yield 82%; m.p. 425–426 K; IR (ATR): = 3179 (m, νNH), 2966 (s, νCH), 2875 (w, νCH), 2828 (w, νCH), 1661 (m, νC=N), 1307 (s, νC–N), 1055 (s , νC=S), 963 (w, νN–N), 647 (m, νC–S) cm^{-1}; ^{1}H NMR (400 MHz, DMSO-d_6): δ = 11.98 (1H, s, NH), 2.55 (2H, m, CH_2), 2.44 (3H, s, CH_3), 2.11 (1H, m, CH), 1.96 (2H, q, CH_2, $^3J_{HH}$ = 4.58 Hz, $^4J_{HH}$ = 3.62 Hz), 1.25 (2H, m, CH_2), 0.95 (3H, s, CH_3), 0.90 (3H, s, CH_3), 0.71 (3H, s, CH_3) ppm; ^{13}C{^{1}H} NMR (100 MHz, DMSO-d_6): δ = 198.24 (C=S), 170.82 (C=N), 52.89 (CN–C–CH_3), 47.57 (CH_3–C–CH_3), 43.35 (CH_2–CH–CH_2), 35.10 (CN–CH_2–CH), 32.21 (CN–C–CH_2), 26.63 (CH_2–CH–CH_2), 19.18 (CH_3–S), 18.43 (CH_3–C–CH_3), 16.79 (CH_3–C–CH_3), 11.07 (CN–C–

Table 1. Crystallographic data and refinement details for compounds **2**, **4** and **5**.

	2	**4**	**5**
Chemical formula	$C_{12}H_{20}N_2S_2$	$C_{12}H_{18}N_2OS_2$	$C_{12}H_{18}N_2S_2$
M_r	256.42	270.40	254.41
Crystal system	Orthorhombic	Monoclinic	Monoclinic
Space group	$P\,2_1\,2_1\,2_1$	$P\,1\,2_1\,1$	$P\,1\,2_1\,1$
Temperature (K)	150	150	150
a (Å)	11.9408 (1)	6.9904 (2)	10.4610 (2)
b (Å)	12.6899 (2)	10.5192 (3)	12.6780 (2)
c (Å)	17.9505 (3)	9.5559 (2)	10.7956 (2)
α (°)	90	90	90
β (°)	90	101.2630 (1)	108.8900 (10)
γ (°)	90	90	90
V (Å^3)	2720.00 (7)	689.15 (3)	1354.65 (4)
Z	8	2	4
D_{calc} (g cm^{-3})	1.252	1.303	1.247
μ (Mo$K\alpha$, mm^{-1})	0.369	0.373	0.370
F(000)	1104	288	544
θ_{min}, θ_{max} (°)	5.112, 27.483	5.106, 27.488	5.127, 27.460
No. of reflections collected	6197	2789	5898
No. of independent reflections	6197	2789	5898
No. of reflections $I > 2\sigma(I)$	5414	2566	5215
Parameters refined	305	162	319
R_1 [$F^2 > 2\sigma(F^2)$]	0.0362	0.0307	0.0366
$wR(F^2)$, all data	0.0890	0.0699	0.0875
S	1.058	1.054	1.053
$\Delta\rho_{max}$, $\Delta\rho_{min}$ (e$Å^{-3}$)	0.239, –0.252	0.189, –0.183	0.211, –0.250

CH_3) ppm; UV/Vis (1×10^{-4} M, DMSO): λ_{max} (ε) = 350 (394.5), 304 (20909), 273 (10783); MS (EI, 70 eV) m/z (%): 256 (8.2) [M]$^+$, 183 (100); $C_{12}H_{20}N_2S_2$: (calc) C 56.21, H 7.86, N 10.92, (found) C 56.02, H 7.73, N 10.96.

2.3.2. Methyl (E)-2-((1S,4S)-1,7,7-trimethylbicyclo[2.2.1]heptan-2-ylidene)hydrazine-1-carbodithioate, SMSCM (**2**). White powder; yield 80%; m.p. 425–426 K; ; IR (ATR): = 3177 (m, νNH), 2964 (s, νCH), 2877 (w, νCH), 2836 (w, νCH), 1660 (m, νC=N), 1303 (s, νC–N), 1047 (s , νC=S), 952 (w, νN–N), 636 (m, νC–S) cm^{-1}; ^{1}H NMR (400 MHz, DMSO-d_6): δ = 11.98 (1H, s, NH), 2.55 (2H, m, CH_2), 2.44 (3H, s, CH_3), 2.11 (1H, m, CH), 1.96 (2H, q, CH_2, $^3J_{HH}$ = 4.58 Hz, $^4J_{HH}$ = 3.62 Hz), 1.25 (2H, m, CH_2) 0.95 (3H, s, CH_3), 0.90 (3H, s, CH_3), 0.71 (3H, s, CH_3) ppm; ^{13}C{^{1}H} NMR (100 MHz, DMSO-d_6): δ = 198.27 (C=S), 170.86 (C=N), 52.92 (CN–C–CH_3), 47.61 (CH_3–C–CH_3), 43.38 (CH_2–CH–CH_2), 35.13 (CN–CH_2–CH), 32.23 (CN–C–CH_2), 26.66 (CH_2–CH–CH_2), 19.20 (CH_3–S), 18.46 (CH_3–C–CH_3), 16.81 (CH_3–C–CH_3), 11.11 (CN–C–CH_3) ppm; UV/Vis (1×10^{-4} M, DMSO): λ_{max} (ε) = 350 (449), 304 (20981), 272 (10746); MS (EI, 70 eV) m/z (%): 256 (4.4) [M]$^+$, 183 (100); $C_{12}H_{20}N_2S_2$: (calc.) C 56.21, H 7.86, N 10.92, (found) C 56.06, H 7.38, N 11.04.

2.3.3. Methyl (Z)-2-((1S,4R)-4,7,7-trimethyl-3-oxobicyclo[2.2.1]heptan-2-ylidene)hydrazine-1-carbodithioate, SMRCQ (**3**). Yellow powder, yield 75%; m.p. 377–378 K; IR (ATR): = 3232 (m, νNH), 2958 (s νCH), 2942 (m, νCH), 2879 (w, νCH), 1713 (s, νC=O), 1607 (m, νC=N), 1263 (s, νC–N), 1088 (s , νC=S), 981 (w, νN–N), 657 (m, νC–S) cm^{-1}; ^{1}H NMR (400 MHz, DMSO-d_6): δ = 12.74 (1H, s, NH), 3.51 (1H, t, CH, $^3J_{HH}$ = 4.6 Hz, $^3J_{HH}$ = 3.7 Hz), 2.50 (3H, s, CH_3), 1.91 (2H, m, CH_2), 1.42 (2H, m, CH_2), 0.97 (3H, s, CH_3), 0.93 (3H, s, CH_3), 0.77 (3H, s, CH_3) ppm; ^{13}C{^{1}H} NMR (100 MHz, DMSO-d_6): δ = 204.53 (C=S), 203.02 (C=O), 154.75 (C=N), 57.94 (CO–C–CH_3), 48.29 (CN–CH–CH_2), 44.48 (CH_3–C–CH_3), 29.83 (CO–C–CH_2), 23.75 (CN–CH–CH_2), 20.37 (CH_3–S), 17.40 (CH_3–C–CH_3), 17.24 (CH_3–C–CH_3), 9.03 (CO–C–CH_3) ppm; UV/Vis (1×10^{-4} M, DMSO): λ_{max} (ε) = 393.5 (11730), 332.5 (12097), 265.5 (5645); MS (EI, 70 eV) m/z (%): 270 (4.7) [M]$^+$, 159 (100); $C_{12}H_{18}N_2OS_2$: (calc.) C 53.30, H 6.71, N 10.36, (found) C 52.17, H 6.64, N 10.93.

2.3.4. Methyl (Z)-2-((1R,4S)-4,7,7-trimethyl-3-oxobicyclo[2.2.1]heptan-2-ylidene)hydrazine-1-carbodithioate, SMSCQ (**4**). Yellow powder; yield 75%; m.p. 377–378 K, IR (ATR): = 3244 (m, νNH), 2960 (s, νCH), 2942 (m, νCH), 2874 (w, νCH), 1713 (s, νC=O), 1606 (m, νC=N), 1265 (s, νC–N), 1088 (s , νC=S), 979 (w, νN–N), 655 (m, νC–S) cm^{-1}; ^{1}H NMR (400 MHz, DMSO-d_6): δ = 12.75 (1H, s, NH), 3.51 (1H, t, CH, $^3J_{HH}$=4.6 Hz, $^3J_{HH}$=3.7 Hz), 2.50 (3H, s, CH_3), 1.91 (2H, m, CH_2), 1.43 (2H, m, CH_2), 0.97 (3H, s, CH_3), 0.94 (3H, s, CH_3), 0.77 (3H, s, CH_3) ppm; ^{13}C{^{1}H} NMR (100 MHz, DMSO-d_6): δ = 204.55 (C=S), 203.03 (C=O), 154.77 (C=N), 57.96 (CO–C–CH_3), 48.30 (CN–CH–CH_2), 44.49 (CH_3–C–CH_3), 29.83 (CO–C–CH_2), 23.76 (CN–CH–CH_2), 20.39 (CH_3–S), 17.41 (CH_3–C–CH_3), 17.27 (CH_3–C–CH_3), 9.05 (CO–C–CH_3) ppm; UV/Vis (1×10^{-4} M, DMSO): λ_{max} (ε) = 394.2 (12273), 333.0 (12846), 266.5 (6017); MS (EI, 70 eV) m/z (%): 270 (1.1) [M]$^+$, 159 (100); $C_{12}H_{18}N_2OS_2$: (calc.) C 53.30, H 6.71, N 10.36, (found) C 51.87, H 6.52, N 10.27.

2.3.5. Benzyl (E)-2-((1R,4R)-1,7,7-trimethylbicyclo[2.2.1]heptan-2-ylidene)hydrazine-1-carbodithioate, SBRCM (**7**). White powder; yield 85%; m.p. 387–388 K; IR (ATR): = 3189 (m, νNH), 2952 (m, νCH), 2900 (w, νCH), 1652 (m, νC=N), 1307 (s, νC–N), 1033 (s , νC=S), 963 (w, νN–N), 629 (m, νC–S) cm^{-1}; ^{1}H NMR (400 MHz, DMSO-d_6): δ = 12.04 (1H, s, NH), 7.40 (2H, d, *ortho*-CH, $^3J_{HH}$ = 7.36 Hz), 7.32 (1H, m, *para*-CH), 7.28 (2H, t, *meta*-CH, $^3J_{HH}$ = 7.28 Hz), 4.42 (2H, s, S–CH_2), 2.56 (2H, m, CH_2), 2.12 (1H, m, CH), 1.95 (2H, q, CH_2, $^3J_{HH}$ = 4.52 Hz, $^3J_{HH}$ = 3.70 Hz), 1.24 (2H, m, CH_2), 0.90 (3H, s, CH_3), 0.89 (3H, s, CH_3), 0.70 (3H, s, CH_3) ppm; ^{13}C{^{1}H} NMR (100 MHz, DMSO-d_6): δ = 196.50 (C=S), 171.18 (C=N), 137.19 (*ipso*-C), 129.15 (2C, *ortho*-C), 128.51 (2C, *meta*-C), 127.10 (*para*-C), 52.94 (CN–C–CH_3), 47.60 (CH_3–C–CH_3), 43.34 (CH_2–CH–CH_2), 37.55 (CH_2–S), 35.16 (CN–CH_2–CH), 32.18 (CN–C–CH_2), 26.60 (CH_2–CH–CH_2), 19.18 (CH_3–C–CH_3), 18.40 (CH_3–C–CH_3), 11.07 (CN–C–CH_3) ppm; UV/Vis (1×10^{-4} M, DMSO): λ_{max} (ε) =346 (1454), 307 (18667), 275 (12502); MS (EI, 70 eV) m/z (%): 332 (0.8) [M]$^+$, 91 (100); $C_{18}H_{24}N_2S_2$: (calc.) C 65.02, H 7.27, N 8.42, (found) C 64.49, H 7.14, N 8.23.

2.3.6. Benzyl (E)-2-((1S,4S)-1,7,7-trimethylbicyclo[2.2.1]heptan-2-ylidene)hydrazine-1-carbodithioate, SBSCM (**8**). White powder; yield 85%; m.p. 387–388 K; IR (ATR): = 3192 (m, νNH), 2953 (m, νCH), 2900 (w, νCH), 1652 (m, νC=N), 1306 (s, νC–N), 1045 (s , νC=S), 958 (w, νN–N), 629 (m, νC–S) cm^{-1}; ^{1}H NMR (400 MHz, DMSO-d_6): δ = 12.04 (1H, s, NH), 7.39 (2H, d, *ortho*-CH, $^3J_{HH}$ = 7.4 Hz), 7.32 (1H, m, *para*-CH), 7.29 (2H, t, *meta*-CH, $^3J_{HH}$ = 7.28 Hz), 4.42 (2H, s, S–CH_2), 2.56 (2H, m, CH_2), 2.11 (1H, m, CH), 1.96 (2H, q, CH_2, $^3J_{HH}$ = 4.50 Hz, $^3J_{HH}$ = 3.68 Hz), 1.24 (2H, m, CH_2), 0.90 (3H, s, CH_3), 0.89 (3H, s, CH_3), 0.70 (3H, s, CH_3) ppm; ^{13}C{^{1}H} NMR (100 MHz, DMSO-d_6): δ = 196.51 (C=S), 171.21 (C=N), 137.20 (*ipso*-C), 129.24 (2C, *ortho*-C), 128.47 (2C, *meta*-C), 127.12 (*para*-C), 52.97 (CN–C–CH_3), 47.61 (CH_3–C–CH_3), 43.35 (CH_2–CH–CH_2), 37.56 (CH_2–S), 35.18 (CN–CH_2–CH), 32.20 (CN–C–CH_2), 26.61 (CH_2–CH–CH_2), 19.19 (CH_3–C–CH_3), 18.42 (CH_3–C–CH_3), 11.10 (CN–C–CH_3) ppm; UV/Vis (1×10^{-4} M, DMSO): λ_{max} (ε) =346 (1418), 306 (18693), 276 (12507); MS (EI, 70 eV) m/z (%): 332 (3.2) [M]$^+$, 91 (100); $C_{18}H_{24}N_2S_2$: (calc.) C 65.02, H 7.27, N 8.42, (found) C 64.17, H 7.03, N 8.26.

2.3.7. Benzyl (Z)-2-((1S,4R)-4,7,7-trimethyl-3-oxobicyclo[2.2.1]heptan-2-ylidene)hydrazine-1-carbodithioate, SBRCQ (**9**). Yellow powder; yield 70%; m.p. 417–418 K; IR (ATR): = 3248 (m, νNH), 2964 (m, νCH), 2908 (w, νCH), 1707

(s, νC=O), 1605 (m, νC=N), 1268 (s, νC–N), 1062 (s , νC=S), 987 (w, νN–N), 660 (m, νC–S) cm^{-1}; ^{1}H NMR (400 MHz, DMSO-d_6): δ = 12.81 (1H, s, NH), 7.40 (2H, d, *ortho*-CH, $^3J_{HH}$ = 7.36 Hz), 7.32 (1H, m, *para*-CH), 7.29 (2H, t, *meta*-CH, $^3J_{HH}$ = 7.20 Hz), 4.43 (2H, s, S–CH_2), 3.50 (1H, t, $^3J_{HH}$ = 4.58 Hz, $^3J_{HH}$ = 3.71 Hz), 1.91 (2H, m, CH_2), 1.42 (2H, m, CH_2), 0.96 (3H, s, CH_3), 0.92 (3H, s, CH_3), 0.76 (3H, s, CH_3) ppm; ^{13}C{^{1}H} NMR (100 MHz, DMSO-d_6): δ = 204.49 (C=S), 201.11 (C=O), 154.94 (C=N), 136.45 (*ipso*-C), 129.18 (2C, *ortho*-C), 128.48 (2C, *meta*-C), 127.29 (*para*-C), 57.96 (CO–C–CH_3), 48.34 (CN–CH–CH_2), 44.50 (CH_3–C–CH_3), 37.95 (CH_2–S), 29.82 (CO–C–CH_2), 23.76 (CN–CH–CH_2), 20.41 (CH_3–C–CH_3), 17.40 (CH_3–C–CH_3), 9.04 (CO–C–CH_3) ppm; UV/Vis (1×10^{-4} M, DMSO): λ_{max} (ε) =390.5 (5774), 330.5 (9275), 299.5 (7496), 266.5 (7570); MS (EI, 70 eV) m/z (%): 346 (21.7) $[M]^+$, 91 (100); $C_{18}H_{22}N_2OS_2$: (calc.) C 62.39, H 6.4, N 8.08, (found) C 62.41, H 6.23, N 7.94.

2.3.8. Benzyl (Z)-2-((1R,4S)-4,7,7-trimethyl-3-oxobicyclo[2.2.1]heptan-2-ylidene)hydrazine-1-carbodithioate, SBSCQ (**10**). Yellow powder; yield 75%; m.p. 417–418 K; IR (ATR): = 3247 (m, νNH), 2962 (m, νCH), 2901 (w, νCH), 1706 (s, νC=O), 1605 (m, νC=N), 1269 (s, νC–N), 1098 (s , νC=S), 994 (w, νN–N), 661 (m, νC–S) cm^{-1}; ^{1}H NMR (400 MHz, DMSO-d_6): δ = 12.79 (1H, s, NH), 7.39 (2H, d, *ortho*-CH, $^3J_{HH}$ = 7.36 Hz), 7.32 (1H, m, *para*-CH), 7.29 (2H, t, *meta*-CH, $^3J_{HH}$ = 7.20 Hz), 4.44 (2H, s, S–CH_2), 3.51 (1H, t, $^3J_{HH}$ = 4.58 Hz, $^3J_{HH}$ = 3.72 Hz), 1.92 (2H, m, CH_2), 1.41 (2H, m, CH_2), 0.92 (3H, s, CH_3), 0.96 (3H, s, CH_3), 0.76 (3H, s, CH_3) ppm; ^{13}C{^{1}H} NMR (100 MHz, DMSO-d_6): δ = 204.42 (C=S), 201.08 (C=O), 154.91 (C=N), 136.43 (*ipso*-C), 129.21 (2C, *ortho*-C), 128.44 (2C, *meta*-C), 127.24 (*para*-C), 57.91 (CO–C–CH_3), 48.33 (CN–CH–CH_2), 44.44 (CH_3–C–CH_3), 37.91 (CH_2–S), 29.78 (CO–C–CH_2), 23.72 (CN–CH–CH_2), 20.37 (CH_3–C–CH_3), 17.36 (CH_3–C–CH_3), 8.99 (CO–C–CH_3) ppm; UV/Vis (1×10^{-4} M, DMSO): λ_{max} (ε) =389.5 (7241), 299.5 (12385), 300.5 (9276), 266.5 (8753); MS (EI, 70 eV) m/z (%): 346 (9.1) $[M]^+$, 91 (100); $C_{18}H_{22}N_2OS_2$: (calc.) C 62.39, H 6.4, N 8.08, (found) C 61.48, H 6.17, N 8.15.

2.4. General procedure for the preparation of compounds 5–6 and 11–12

The synthesis was similar to the rest of the compounds except that 1 mL of diluted HCl (1 M) was used and the reaction was conducted at room temperature.

2.4.1. Methyl (R,E)-2-(2-methyl-5-(prop-1-en-2-yl)cyclohex-2-en-1-ylidene)hydrazine-1-carbodithioate, SMRCV (**5**). Pale yellow powder; yield 87%; m.p. 391–393 K; IR (ATR): = 3155 (m, νNH), 2962 (m, νCH), 2925 (m, νCH), 2869 (w, νCH), 1640 (w, νC=N), 1587 (w, νC=C), 1326 (s, νC–N), 1061 (s , νC=S), 964 (w, νN–N), 632 (m, νC–S) cm^{-1}; ^{1}H NMR (400 MHz, DMSO-d_6): δ = 12.34 (1H, s, NH), 6.29 (1H, s, CH), 4.78 (2H, d, CH_2, $^3J_{HH}$ = 6.4 Hz), 3.02 (1H, m, CH), 2.44 (3H, s, CH_3), 2.31 (2H, m, CH_2), 2.10 (2H, m, CH_2), 1.82 (3H, s, CH_3), 1.73 (3H, s, CH_3) ppm; ^{13}C{^{1}H} NMR (100 MHz, DMSO-d_6): δ = 199.73 (C=S), 153.45 (C=N), 147.44 (CN–C=CH), 136.21 (CN–C=CH), 131.95 (CH–C=CH_2), 110.21 (CH–C=CH_2), 38.90 (CH–C=CH_2), 30.23 (CH_2–CH–CH_2), 29.79 (CH_2–CH–CH_2), 20.74 (CH_3–S), 17.54 (CN–C–CH_3), 17.0 (CH–C–CH_3) ppm; UV/Vis (1×10^{-4} M, DMSO): λ_{max} (ε) = 340.5 (17786), 323.4 (21738), 278.1 (6194); MS (EI, 70 eV) m/z (%): 254 (36.8) $[M]^+$, 91 (100); $C_{12}H_{18}N_2S_2$: (calc.) C 56.65, H 7.13, N 11.01, (found) C 55.43, H 7.21, N 10.04.

2.4.2. Methyl (S,E)-2-(2-methyl-5-(prop-1-en-2-yl)cyclohex-2-en-1-ylidene)hydrazine-1-carbodithioate SMSCV (**6**). Pale yellow powder; yield 80%; m.p. 391–393 K; IR (ATR): = 3158 (m, νNH), 2973 (w, νCH), 2953 (m, νCH), 2922 (w, νCH), 2877 (w, νCH), 1640 (w, νC=N), 1585 (w, νC=C), 1325 (s, νC–N), 1061 (s , νC=S), 962 (w, νN–N), 637 (m, νC–S) cm^{-1}; ^{1}H NMR (400 MHz, DMSO-d_6): δ = 12.34 (1H, s, NH), 6.29 (1H, s, CH), 4.78 (2H, d, CH_2, $^3J_{HH}$ = 6.4 Hz), 3.02 (1H, m, CH), 2.44 (3H, s, CH_3), 2.30 (2H, m, CH_2), 2.10 (2H, m, CH_2), 1.82 (3H, s, CH_3), 1.73 (3H, s, CH_3), ppm; ^{13}C{^{1}H} NMR (100 MHz, DMSO-d_6): δ = 199.73 (C=S), 153.42 (C=N), 147.43 (CN–C=CH), 136.20 (CN–C=CH), 131.97 (CH–C=CH_2), 110.21 (CH–C=CH_2), 38.88 (CH–C=CH_2), 30.23 (CH_2–CH–CH_2), 29.81 (CH_2–CH–CH_2), 20.73 (CH_3–S), 17.54 (CN–C–CH_3), 17.0 (CH–C–CH_3) ppm; UV/Vis (1×10^{-4} M, DMSO): λ_{max} (ε) = 341.2 (18367), 322.1 (22546), 279.5 (6827); MS (EI, 70 eV) m/z (%): 254 (57.0) $[M]^+$, 91.1 (100); $C_{12}H_{18}N_2S_2$: (calc.) C 56.65, H 7.13, N 11.01, (found) C 55.37, H 7.02, N 10.87.

2.4.3. Benzyl (R,E)-2-(2-methyl-5-(prop-1-en-2-yl)cyclohex-2-en-1-ylidene)hydrazine-1-carbodithioate SBRCV (**11**). Pale yellow powder; yield 65%; m.p. 405–406 K; IR (ATR): =3184 (m, νNH), 2921 (m, νCH), 2868 (w, νCH), 1642 (w, νC=N), 1588 (w, νC=C), 1315 (s, νC–N), 1060 (s , νC=S), 974 (w, νN–N), 634 (m, νC–S) cm^{-1}; ^{1}H NMR (400 MHz, DMSO-d_6): *δ* = 12.42 (1H, s, NH), 7.39 (2H, d, *ortho*-CH, $^3J_{HH}$ = 7.32 Hz), 7.32 (1H, m, *para*-CH), 7.29 (2H, t, *meta*-CH, $^3J_{HH}$ = 7.16 Hz), 6.30 (1H, s, CH), 4.80 (2H, d, CH_2, $^3J_{HH}$ = 6.4 Hz), 4.44 (2H, s, S–CH_2), 3.04 (1H, m, CH), 2.32 (2H, m, CH_2), 2.12 (2H, m, CH_2), 1.79 (3H, s, CH_3), 1.75 (3H, s, CH_3) ppm; ^{13}C{^{1}H} NMR (100 MHz, DMSO-d_6): *δ* = 197.79 (C=S), 153.77 (C=N), 147.32 (CN–C=CH), 137.12 (*ipso*-C), 136.38 (CN–C=CH), 131.79 (CH–C=CH_2), 129.17 (2C, *ortho*-C), 128.42 (2C, *meta*-C), 127.08 (*para*-C), 110.11 (CH–C=CH_2), 39.99 (CH–C=CH_2), 37.57 (CH_2–S), 30.19 (CH_2–CH–CH_2), 29.69 (CH_2–CH–CH_2), 20.64 (CN–C–CH_3), 17.43 (CH–C–CH_3) ppm; UV/Vis (1×10^{-4} M, DMSO): λ_{max} (ε) =327.0 (20536), 287.0 (10013); MS (EI, 70 eV) *m/z* (%): 330 (7.3) $[M]^+$,91 (100); $C_{18}H_{22}N_2S_2$: (calc.) C 65.41, H 6.71, N 8.48, (found) C 65.45, H 6.54, N 9.54.

2.4.4. Benzyl (S,E)-2-(2-methyl-5-(prop-1-en-2-yl)cyclohex-2-en-1-ylidene)hydrazine-1-carbodithioate SBSCV (**12**). Pale yellow powder; yield 68%; m.p. 405–406 K; IR (ATR): = 3189 (m, νNH), 2924 (m, νCH), 2860 (w, νCH), 1643 (w, νC=N), 1585 (w, νC=C), 1314 (s, νC–N), 1059 (s , νC=S), 970 (w, νN–N), 634 (m, νC–S) cm^{-1}; ^{1}H NMR (400 MHz, DMSO-d_6): δ = 12.40 (1H, s, NH), 7.39 (2H, d, *ortho*-CH, $^{3}J_{HH}$ = 7.32 Hz), 7.32 (1H, m, *para*-CH), 7.29 (2H, t, *meta*-CH, $^{3}J_{HH}$ = 7.18 Hz), 6.30 (1H, s, CH), 4.80 (2H, d, CH_2, $^{3}J_{HH}$ = 6.4 Hz,), 4.45 (2H, s, S–CH_2), 3.04 (1H, m, CH), 2.32 (2H, m, CH_2), 2.12 (2H, m, CH_2), 1.80 (3H, s, CH_3), 1.76 (3H, s, CH_3) ppm; ^{13}C{^{1}H} NMR (100 MHz, DMSO-d_6): δ = 197.79 (C=S), 153.77 (C=N), 147.32 (CN–C=CH), 137.12 (*ipso*-C), 136.26 (CN–C=CH), 131.83 (CH–C=CH_2), 129.16 (2C, *ortho*-C), 128.55 (2C, *meta*-C), 127.17 (*para*-C), 110.28 (CH–C=CH_2), 40.19 (CH–C=CH_2), 37.64 (CH_2–S), 30.20 (CH_2–CH–CH_2), 29.01 (CH_2–CH–CH_2), 20.52 (CN–C–CH_3), 17.54 (CH–C–CH_3) ppm; UV/Vis (1×10^{-4} M, DMSO): λ_{max} (ε) =330.2 (8724), 290.8 (9812); MS (DI, 70 eV) m/z (%): 330 (3.6) $[M]^{+}$,91 (100); $C_{18}H_{22}N_2S_2$: (calc.) C 65.41, H 6.71, N 8.48, (found) C 63.73, H 6.54, N 8.23.

2.5. Virus and cells for antiviral evaluation

Aedes albopictus clone C6/36 cells were maintained to propagate the dengue virus type 2 (DENV 2); African green monkey (*Chlorocebus* sp.) kidney Vero cells were grown for antiviral analysis. Both cells were grown in Eagle's Minimum Essential Medium (EMEM) (Biowest LLC, Riverside, MO, USA) with 10% Fetal Bovine Serum (FBS) (Biowest LLC).

Ribavirin tablets (Copegus, 200 mg, Genentech, Inc., South San Francisco, CA, USA) were purchased and stock solutions were stored. Dilutions were prepared in 2% FBS (maintenance media) at the time of assay. TCID50 assay was employed to measure the titer of the virus stocks for antiviral evaluation following standard methods [25]. The viral CPE was observed on the third and fourth days and observations were recorded based on the Reed–Muench method.

2.5.1. MTT cytotoxicity assay

The 96-well plates were seeded with 100 µL of Vero cell suspension at a density of 1 × 105 cells / mL and the next day were treated with different dilutions of the synthesized compounds. Control wells were treated with only the vehicle media used to prepare the antiviral dilutions. Plates were incubated for four days at 37 °C. Following the addition of 15 µL of MTT (Sigma-Aldrich Corp., St. Louis, MO, USA) solution into each well, the plates were incubated at 37 °C for another 4 h. Subsequently, the medium was carefully aspirated from all the wells and 100 µL of DMSO was added to each well [26]. The optical density (OD) of the wells was measured at 570 nm using a 96-well plate reader (Tecan Group AG, Männedorf, Switzerland). The percentage cell viability was calculated against the untreated controls. Dose-response curves were plotted. Half maximal cytotoxic concentration (CC50) was calculated using Graph Pad Prism for Windows, Version 5 (GraphPad Software Inc., San Diego, CA, USA).

2.5.2. CPE reduction-based antiviral assay

Plates were seeded with Vero cell suspension (100 µL) at a density of 1 × 105 cells/mL one day before the wells were treated with TCID50 (100 µL) dilution of the DENV 2 stock and untreated control wells were maintained in parallel. After 1 h of viral adsorption, unbound viruses were washed and different antiviral dilutions were added. These plates were further incubated for 4 more days and were observed daily [26,27]. Observations were recorded on the third and fourth days. The wells were marked for CPE reduction according to the grading system defined by Kudi and Myint [28].

2.5.3. Foci forming unit reduction assay (FFURA)

Antiviral activity was quantitatively validated by measuring the reduction in the number of DENV infectious foci after 4 days of treatment. DENV 2 infected Vero cells were treated with different antiviral dilutions supplemented with 2% FBS and 1.5% carboxymethyl cellulose (CMC). Virus foci were stained and visualized according to the published protocol [29]. The number of foci was counted through stereomicroscope and virus titer was stated as foci forming unit (FFU). To calculate the antiviral activity of antidengue compounds, the percentage reduction in foci (%RF) was calculated between the treated, and untreated wells maintained in parallel. The assay was repeated three times, dose-response curves were plotted and half minimal inhibitory concentration (IC50) and selectivity index (SI) were calculated.

3. Results and discussion

3.1. Chemistry

3.1.1. Synthesis and spectroscopic characterization of compounds 1–4, and 7–10

Conventionally, the formation of Schiff bases involving SMDTC or SBDTC is rather facile without much reliance on factors such as temperature, pH, and catalytic reagents [30]. In this study, however, the condensation reaction did not take place even after prolonged reflux at elevated temperature. A plausible reason for the failure of the reaction is that the structurally rigid bicyclic ring of the monoterpenes (camphor and camphorquinone in particular) coupled with the weakened dipole moment and reduced electrophilicity of the carbonyl carbon might have inhibited the reactivity by

preventing nucleophilic attack from the electronegative S-substituted dithiocarbazates. One possible way to circumvent the inertness of the reaction is through capitalization of the electro negativity of the carbonyl oxygen by introducing a Lewis acid such as hydrogen ion to activate the nucleophilic oxygen.

IR analysis shows the presence of some essential peaks at about 3150–3250 cm^{-1} and 1605–1660 cm^{-1} which can be attributed to secondary νN–H and νC=N peaks. The difference between the νN–H peaks and the two distinctive peaks characteristic of asymmetric and symmetric stretching of primary amines as observed for SM- and SBDTC, as well as the absence of νC = N in the spectra of the precursors imply that condensation has indeed taken place between the dithiocarbazates and monoterpenes. While the disappearance of νC=O frequency in SMRCM, SMSCM, SBRCM, and SBSCM is further evidence which confirms the formation of the Schiff bases, the peak is still observed at 1706–1713 cm^{-1} in the corresponding spectra of SMRCQ, SMSCQ, SBRCQ, and SBSCQ and it is more resolved compared to the broad asymmetric C=O peak of the starting precursor (i.e. camphorquinone) at ca. 1745 cm^{-1}. This suggests that only one of the C = O groups reacted with the substituted dithiocarbazates, while the other C=O which is likely the one adjacent to the methyl group, remains intact due to steric hindrance. νC=S at 1030–1100 cm^{-1} together with the absence of νS–H (2600–2700 cm^{-1}) are clear evidence that the solid Schiff bases are predominantly in their thione tautomeric form [31].

^{1}H NMR spectra in DMSO-d_6 show thionamide N–H peaks for SMRCM, SMSCM, SBRCM, and SBSCM at 11.98–12.04 ppm, which is within the typical range for *E*-configuration along the C=N imine bond [32]. SMRCQ, SMSCQ, SBRCQ, and SBSCQ Schiff bases exhibit a resonance for the thionamide proton between 12.71–12.81 ppm indicating *Z*-configuration (Figure 1a). Such configuration enables an intramolecular interaction between thionamide, and unreacted carbonyl groups resulting in the relatively high field chemical shift for the thionamide proton (Figure 1b). As expected, all Schiff bases remain in the thione tautomeric form even in a polar solvent like DMSO with no signal assignable to thiol proton being seen near 4 ppm [32]. The thione form of a dithiocarbazate Schiff base has been found to be more stable than its thiol counterpart by 14.5 kJ/mol through gas phase DFT calculation [33]. For the rest of the protons and carbon nuclei, their resonances appear in the typical range, and assignment has been unambiguously determined upon comparison with the ^{1}H and $^{13}C\{^{1}H\}$ NMR spectra of the corresponding precursors (cf. Section 2.3. and 2.4.).

3.1.2. Synthesis and spectroscopic characterization of compounds 5–6, and 11–12

Since the enantiomeric carvones did not react with the substituted dithiocarbazates under the heat-and-reflux routine commonly used, acid was used to catalyze the reaction. However, the additional alkene functional group in carvone makes it susceptible to acid addition leading to undesired stereoisomerization or racemization of the enantiomerically pure reagents (see Scheme 2).

To reduce the possibility of the occurrence of the undesired side reactions, a catalytic amount of dilute acid was used and, in addition, the synthesis was conducted at room temperature even though the condensation reaction, being an endothermic process, would have been favored by higher temperatures [34]. IR spectra of the carvone-DTC Schiff bases possess a profile similar to that of their camphor- and camphorquinone-DTC counterparts implying that the Schiff bases

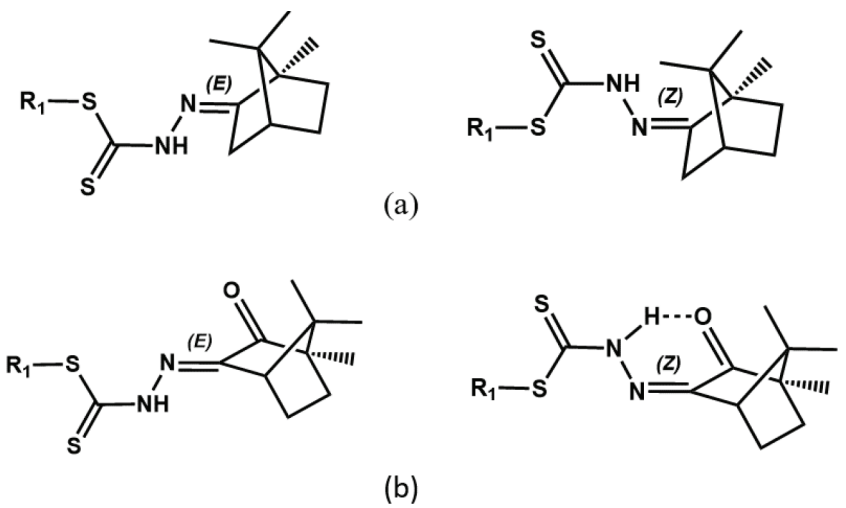

Figure 1 The *EZ*-configuration for (a) compounds **1**, **2**, **5** and **6** with all compounds primarily appearing in the *E*-configuration, (b) compounds **3**, **4**, **7** and **8** with all mainly appearing in the *Z*-configuration.

were successfully synthesized through acid-catalyzed condensation. More importantly, the presence of ν(C=C) at ca. 1582 cm^{-1} together with the absence of an intense ν(C-Cl) peak (~700 cm^{-1}) prove that the acid addition reaction did not take place.

The thionamide protons in these compounds exhibit a resonance between 12.38 and 12.43 ppm which is close to those observed for the camphor-DTC Schiff bases indicating that they too adopt an *E*-configuration (Figure 2) along the C=N bond [32]. However, given that the substituted dithiocarbazate fragment is sterically less hindered about the N–N single bond compared to the bulkier camphor-DTC Schiff bases, the possibility of the formation of the *Z*-configuration, generated by flipping towards either side of the monocyclic ring of carvone, cannot be totally omitted. These compounds also display no sign of thione-thiol tautomerism in DMSO solution. The intactness of the alkene groups in the Schiff bases is confirmed by the $^{13}C\{^1H\}$ resonances at 136.34–148.00 ppm that are very close to those observed for the carvone precursors (142.70–143.82 ppm). In addition, there is no trace of any resonance signal for C-Cl at 50–75 ppm which would be expected if addition reaction occurred at the C=C.

The supplementary materials include the IR, EI-MS, ^1H, and $^{13}C\{^1H\}$ NMR Spectra. Supplementary materials Figures S1–S3 are the IR and EI-MS spectra of compounds SMRCM, SMSCM, SBRCM, and SBSCM while, Figures S4–S11 are the ^1H and $^{13}C\{^1H\}$ NMR Spectra of compounds SMRCM, SMSCM, SBRCM, and SBSCM. Figures S12–S14 are the IR and EI-MS spectra of compounds SMRCQ, SMSCQ, SBRCQ, and SBSCQ while, Figures S15–S22 are the ^1H and $^{13}C\{^1H\}$ NMR Spectra of compounds SMRCQ, SMSCQ, SBRCQ, and SBSCQ. Figures S23–S25 are the IR and EI-MS spectra of compounds SMRCV, SMSCV, SBRCV, and SMSCV while, Figures S26–S33 are the ^1H and $^{13}C\{^1H\}$ NMR Spectra of compounds SMRCV, SMSCV, SBRCV, and SMSCV.

3.2. Crystal structures of SMSCM (2), SMSCQ (4) and SMRCV (5)

Figure 3 shows the ORTEP diagrams of SMSCM, SMSCQ, and SMRCV in which SMSCM (Figure 3a) comprises two molecules while SMSCQ (Figure 3b) contains only a single molecule and SMRCV (Figure 3c) comprises two molecules in the asymmetric unit. Each of the structures constituted of three distinct fragments, i.e. the dithiocarbazate (S_2CN_2),

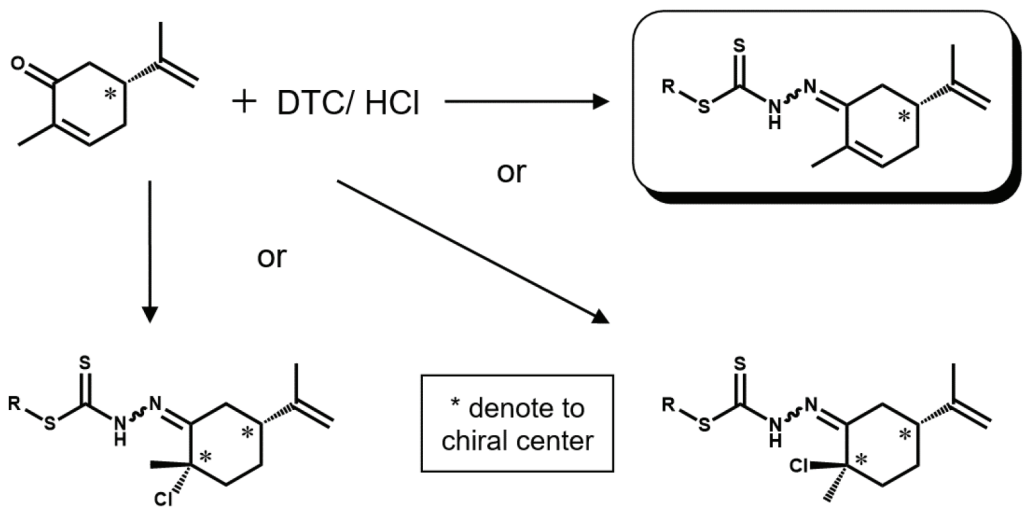

Scheme 2. Possible outcomes of acid catalyzed condensation between carvone and substituted dithiocarbazates.

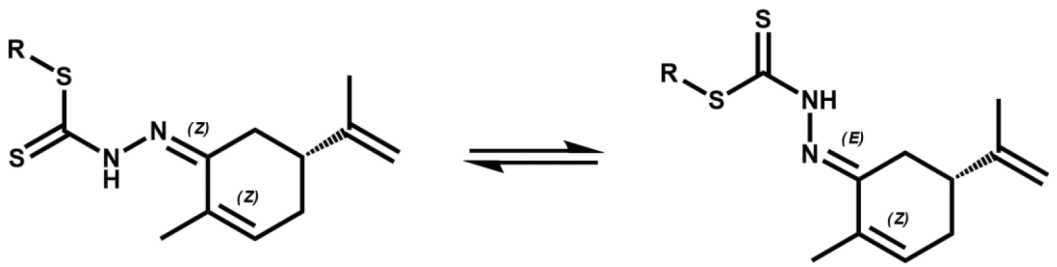

Figure 2. The EZ-configuration for compounds **5**, **6**, **11**, and **12**.

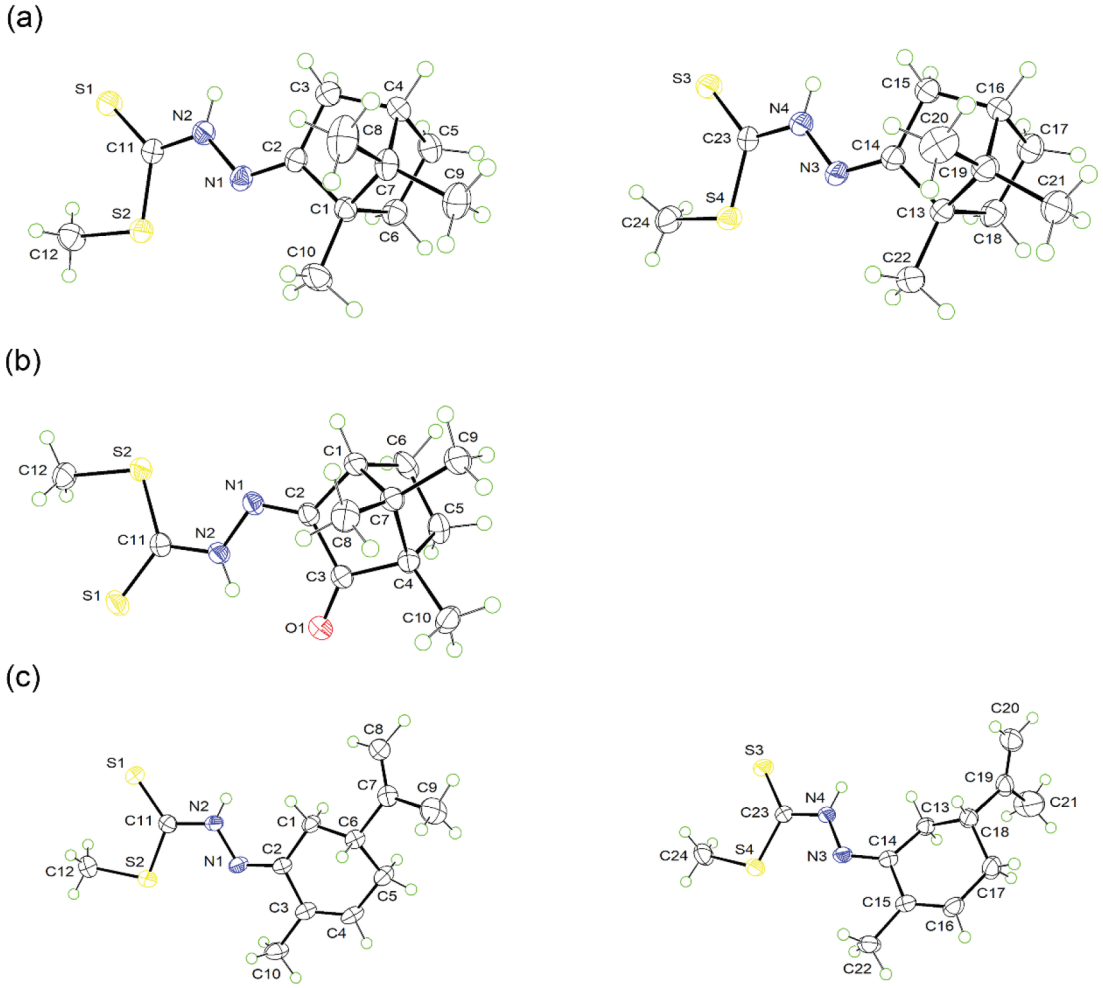

Figure 3. The ORTEP diagram at 50% probability ellipsoids, showing the independent molecule in the asymmetry unit for (a) SMSCM (2), (b) SMSCQ (4) and (c) SMRCV (5).

the appending methyl, and isocyclic ring. The central dithiocarbazate fragment for all structures is essentially planar as shown through the corresponding least-square plane fitting with a r.m.s. deviation of 0.0064 Å and 0.0123 Å for molecule I [S2–C11(S1)–N2–N1] and molecule II [S4–C23(S3)–N4–N3] in SMSCM, 0.0447 Å for SMSCQ as well as 0.0154 Å and 0.0347 Å for molecule I and II in SMRCV. Molecules I and II in SMSCM are slightly differed from each other in that the thiomethyl plane (S1–C11–S2–C12) of the former is relatively less twisted from the central dithiocarbazate plane [S2–C11(S1)–N2–N1] with a dihedral angle of 3.6(1)° as compared to 5.8(1)° for the equivalent planes [S3–C23–S4–C24// S4–C23(S3)–N4–N3] in molecule II. The superimposition of the two molecules results in a r.m.s. deviation of merely 0.073 Å. As for SMRCV, molecules I and II are relatively more deviated from each other with a r.m.s. deviation of the superimposed structures being 0.796 Å. Overall, the least-square plane of thiomethyl (S1–C11–S2–C12 or S3–C23–S4–C24) and isocylic ring (C1–C2–C3–C4–C5–C6 or C13–C14–C15–C16–C17–C18) are twisted from the central dithiocarbazate plane by 14.7(1)° for molecule I and 10.7(1)° for molecule II, respectively.

As consistent with the spectroscopic findings, the solid-state structure of SMSCM and SMRCV appear in *E*–configuration along the C = N imine bond with the torsion angle of –177.5(2) and –176.9(2)° across N2–N1–C2–C1 and N4–N3–C14–C13 for SMSCM as well as –179.1(2) and 178.3(2)° across N2–N1–C2–C3 and N4–N3–C14–C15 for SMRCV, and the same is true for SMSCQ which exists as *Z*– configuration with the torsion angle for N2–N1–C2–C3 being –1.0(4)°. The bond length of C11–S1 (or C23–S3 in the second molecule) for all structures is relatively shorter than C11–S2 or C23–S4 (cf. geometry parameters in Table 2) which reflects the thione character of those DTC Schiff bases. The azine (N2–N1, and N4–N3), and methyl (C12 or C24) residues are respectively arranged in the trans and cis position with respect to thione group (C11=S1 or C23=S3), hence constitute a trans-cis conformation as observed in the

Table 2. Selected geometric parameters (Å, °) for compounds **2**, **4** and **5**.

Parameter	**2**	**4**	**5**
N1–C2	1.277(3)	1.287(3)	1.295(4)
N1–N2	1.395(3)	1.369(3)	1.380(3)
N2–C11	1.340(3)	1.360(3)	1.344(4)
C11–S1	1.663(3)	1.653(3)	1.663(3)
C11–S2	1.762(3)	1.749(2)	1.749(3)
S2–C12	1.795(3)	1.801(3)	1.797(3)
N3–C14	1.273(3)	-	1.285(4)
N3–N4	1.397(3)	-	1.391(3)
N4–C23	1.347(3)	-	1.334(4)
C23–S3	1.668(3)	-	1.672(3)
C23–S4	1.749(3)	-	1.746(3)
S4–C24	1.797(3)	-	1.794(3)
N2–N1–C2	117.3(2)	116.7(2)	118.6(2)
N1–N2–C11	118.7(2)	119.7(2)	118.6(2)
N2–C11–S1	122.0(2)	120.24(19)	121.8(2)
N2–C11–S2	112.96(19)	113.3(2)	112.9(2)
S1–C11–S2	125.04(15)	126.43(17)	125.30(18)
N4–N3–C14	116.5(2)	-	117.5(2)
N3–N4–C23	118.5(2)	-	119.3(2)
N4–C23–S3	121.1(2)	-	121.1(2)
N4–C23–S4	113.6(2)	-	113.4(2)
S3–C23–S4	125.30(16)	-	125.55(17)

majority of DTC Schiff bases in the Cambridge Structural Database [35], with the torsion angles across S1–C11–N2–N1 (or S3–C23–N3–N4), and S1–C11–S2–C12 (or S3–C23–S4–C24) ranged between 171.7(2)°–179.7(1)° and 1.7(3)°–6.8(2)° correspondingly.

In the terms of supramolecular features, the crystal packing of SMSCM and SMRCV are mainly governed by pairwise N–H···S interactions between the molecules in the asymmetric unit leading to the formation of an eight-membered $\{\cdots NHCS\}_2$ homosynthon which is replicated by 2_1 symmetry along all crystallographic directions for the former and along the *b*-plane for the latter, with both showing no directional interactions between those pairs of molecules (Figure 4a). In contrast, SMSCQ is sustained by C–H···O intermolecular interaction between C12–H12A···O1 together with an intramolecular interaction between N2–H2N···O1 leading to CH···O···HN heterosynthon that connects the molecules in a zigzag array, and extends along the *b*-direction (Figure 4b). The molecular packing of SMSCQ were governed by intermolecular C–H···O and intramolecular N–H···O interactions to form a CH···O···HN heterosynthon arranged in a zigzag array along the *b*-direction (Figure 4c). The molecular packing of SMRCV were associated by eight-membered $\{\cdots NHCS\}_2$ homosynthon replicated by 2_1 symmetry along the crystallographic *a* direction (Figure 4d). The stark difference observed in the crystal packing of SMSCQ as compared to SMSCM, or SMRCV is presumably owing to its arrangement in *Z*-configuration which is stabilized by intramolecular N–H···O interaction. It is noteworthy that N–H···O possesses greater interaction energy than N–H···S interaction and hence it might have prevented the formation of the typical eight-membered $\{\cdots NHCS\}_2$ homosynthon as observed in SMSCM, and SMRCV [36]. The geometric parameters characterizing the interactions for the corresponding structures are presented in Table 3.

3.3. Biological assays

3.2.1. MTT-based cytotoxicity and CPE reduction-based primary antiviral evaluation

The compounds did not display strong cytotoxicity. Toxicity decreased in the order carvone (CV) > camphorquinone (CQ) > camphor (CM). All twelve synthetic compounds showed a gradually decreasing trend in CC50 doses (Table 4).

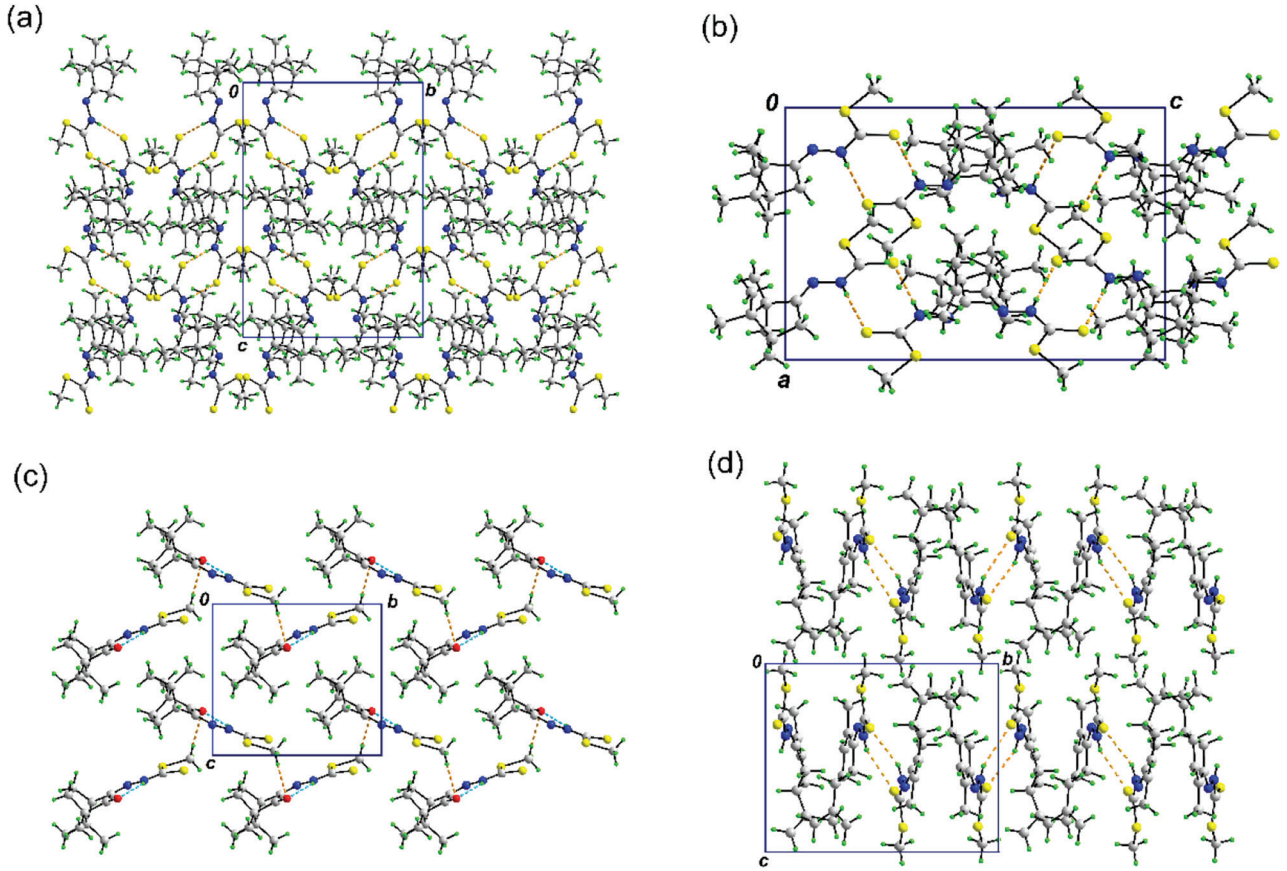

Figure 4. (a) Molecular packing of SMSCM sustained by pairwise N–H···S interaction leading to the formation of eight-membered $\{\cdots NHCS\}_2$ homosynthon related by 2_1 symmetry as view along the crystallographic *a*-direction, (b) a projected view along the *b*-direction, showing the 2_1-symmetry related molecular packing of SMSCM, (c) molecular packing of SMSCQ governed by intermolecular C–H···O (orange dashed line) and intramolecular N–H···O (blue dashed line) interactions to form a CH···O···HN heterosynthon arranged in a zigzag array along the *b*-direction, and (d) molecular packing of SMRCV associated by eight-membered $\{\cdots NHCS\}_2$ homosynthon replicated by 2_1 symmetry along the crystallographic *a* direction.

Table 3. Hydrogen-bond geometry (Å, °) for compounds **2**, **4** and **5**.

D—H···*A*	*D*—H	H···*A*	*D*···*A*	*D*—H···*A*	Symmetry operation
2					
N2—H2N···S3	0.88(3)	2.69(3)	3.557(2)	173(3)	1-*x*, -½ + *y*, ½-*z*
N4—H4N···S1	0.87(4)	2.73(4)	3.602(3)	177(3)	1-*x*, ½ + *y*, ½-*z*
4					
C12—H12A···O1	0.96	2.56	3.516(4)	178	1-*x*, ½ + *y*, 1-*z*
N2—H2N···O1	0.86(4)	2.15(3)	2.801(3)	132(3)	
5					
N2—H2N···S3	0.79(4)	2.71(4)	3.459(3)	159(3)	*x*, *y*, 1 + *z*
N4—H4N···S1	0.90(4)	2.53(5)	3.369(2)	156(4)	1-*x*, ½ + *y*, ½-*z*

The chirality in the form of R and S enantiomers did not show any differential effects on either the cytotoxic dose, or the antiviral activity. The two enantiomers of the compounds showed parallel antidengue potential. Therefore, they may have same pharmacodynamics and can be equally potent. If this is so, the compounds could be used in their enantiomerically pure forms or as a racemic mixture [37]. However, pharmacokinetics of these enantiomers requires further exploration.

Table 4. CC50 doses and degree of CPE reduction in DENV 2-infected Vero cells upon treatment with synthetic Schiff base compounds.

No	Sample ID	M.W	CC50 (μM)	CPE reduction*
1.	SMRCM	256.4	88.4 ± 3.8	++
2.	SMSCM	256.4	88.7 ± 2.0	++
3	SMRCQ	270.4	65.2 ± 4.4	+
4	SMSCQ	270.4	69.2 ± 5.9	+
5	SMRCV	256.4	31.1 ± 8.0	--
6	SMSCV	256.4	24.5 ± 9.2	--
7	SBRCM	332.5	81.7 ± 4.4	++
8	SBSCM	332.5	87.2 ± 5.9	++
9	SBRCQ	346.5	58.4 ± 2.9	--
10	SBSCQ	346.5	58.7 ± 5.1	--
11	SBRCV	332.5	28.5 ± 3.9	+
12	SBSCV	332.5	29.2 ± 6.4	+

* DENV 2 CPE reduction caused by the compound treatments was marked as ++++ for total reduction, +++ for 75% reduction, ++ for 50% reduction, + for less than 50% reduction and -- for no reduction.

The CM compounds showed higher antidengue activity than the other substituted Schiff bases whereas; the CQ and CV compounds were rather more toxic than the CM compounds (Table 2). The DTC-derivatives showed antibiotic potential in a study where some preexisting antibacterial molecules demonstrated greatly enhanced biological activity when conjugated with dithiocarbazate (DTC) [38]. During the present study, camphor compounds showed strong antidengue potential. Camphor is a terpenoid class of biologically active compounds found in the majority of natural products [39]. Camphor is a major component of many essential oils and the biological activities of essential oils are evident [40]. See supplementary materials Figure S34 for dose-response curves and Figures S35a–S35c for CPE-reduction during primary antiviral evaluation.

3.2.2. Foci forming unit reduction (FFUR) based secondary antiviral evaluation

The treatment of Vero cells infected with DENV 2 with three different dilutions of the synthetic compounds revealed reduction in the number of foci appearance for only six of the synthesized compounds, SMRCM, SMSCM, SBRCM, SBSCM, SMRCQ, and SMSCQ. Similarly, the CC50 doses of these compounds (Table 4) were also lower than the six compounds showing viral inhibition during secondary evaluation. This may be due to the cytotoxicity of the compounds during viral foci development that may damage the cells before viral infection [41]. The treatments were compared to the nontreated virus infections incubated parallel. The six potential antiviral compounds were inhibiting the virus in almost a close range of concentration, around 20 μM of the compounds were able to inhibit the virus just about 100%.

The secondary evaluation provided half minimal inhibitory concentrations (IC50) for the six potential antiviral compounds between 6.2 μM and 7.8 μM. Selectivity index (SI) identified the window between the cytotoxic and inhibitory concentrations (Table 5). The SI values were within the range of 8.3 to 14.3, which are very close to each other, therefore, compounds can be considered equally potent. These six compounds were enantiomers of each other and the pattern of inhibition was very similar for each enantiomer of these compounds demonstrating that the antidengue activity might not be the virtue of the chirality of the compounds. See supplementary material, Figure S36 for antidengue effects of ribavirin as a positive control while, and Figures S37a and S37b for the antiviral effects of compounds during secondary evaluation.

4. Conclusion

A series of S-substituted dithiocarbazate Schiff bases containing enantiomeric monoterpenes have been synthesized and their molecular structures were proposed on the basis of elemental analysis and various spectroscopic techniques. To the best of our knowledge, this is the first test of this class of compounds against clinically isolated DENV 2. Compounds have demonstrated strong antiviral potential of varying degree. Secondary evaluation shows that camphor containing compounds may have enhanced potential and should warrant further study.

Table 5. Selectivity index (SI) calculation for the six-potential in vitro antidengue Schiff bases identified after secondary evaluation.

No	Sample ID	CC50 ± SE (μM)	IC50 ± SE (μM)	Selectivity index CC50/IC50
1.	SMRCM	88.4 ± 3.8	6.9 ± 1.2	12.8
2.	SMSCM	88.7 ± 2.0	6.2 ± 3.2	14.3
3.	SMRCQ	65.2 ± 4.4	7.8 ± 3.7	8.3
4.	SMSCQ	69.2 ± 5.9	6.8 ± 2.8	14.1
5.	SBRCM	81.7 ± 4.4	7.8 ± 4.5	10.4
6.	SBSCM	87.2 ± 5.9	6.8 ± 2.3	12.8

Supplementary material

IR spectra, EI-MS spectra, ^{1}H and $^{13}C\{^{1}H\}$ spectra for compound **1**–**12** are provided in an attached supplementary document. Cambridge Crystallographic Data Centre (CCDC) 1947807–1947809 contains the supplementary crystallographic data for compounds **2**, **4,** and **5**. These data can be obtained free of charge from the Cambridge Crystallographic Data Centre through www.ccdc.cam.ac.uk/data_request/cif.

Acknowledgments

Maqsood Maryam gratefully acknowledge Sardar Bahadur Khan Women's University Faculty development project (FDP 2016) for the provision of scholarship for her postgraduate study. Mohamed Ibrahim Mohamed Tahir and Sang Loon Tan are thankful to Dr. D. J. Watkin of the University of Oxford for the access of crystallographic research facilities. The synthesis work was funded by UPM Research University Grant Scheme (RUGS) 05-01-11-1234RU.

Conflict of interest

All Authors declare that they have no conflict of interest.

References

1 World Health Organization. Dengue: guidelines for diagnosis, treatment, prevention and control. Geneva, Switzerland: WHO, 2009.

2 Benelli G, Mehlhorn H. Declining malaria, rising of dengue and Zika virus: insights for mosquito vector control. Parasitology Research 2016; 115 (5): 1747-1754. doi: 10.1007/s00436-016-4971-z

3 Halstead SB. Pathogenesis of dengue: challenges to molecular biology. Science 1988; 239 (4839): 476-481. doi: 10.1126/science.3277268

4 Bhatt S, Gething PW, Brady OJ, Messina JP, Farlow AW et al. The global distribution and burden of dengue. Nature 2013; 496 (1): 504-509. doi: 10.1038/nature12060

5 Liu YT, Lian GD, Yin DW, Su BJ. Synthesis and antimicrobial activity of some novel ferrocene-based Schiff bases containing a ferrocene unit. Research on Chemical Intermediates 2012; 38 (3-5): 1043-1053. doi: 10.1007/s11164-011-0440-6

6 Basha MT, Chartres JD, Pantarat N, Ali MA, Mirza AH et al. Heterocyclic dithiocarbazate iron chelators: Fe coordination chemistry and biological activity. Dalton Transactions 2012; 41 (21): 6536-6548. doi: 10.1039/c2dt12387h

7 Carneiro ZA, Maia PS, Sesti-Costa R, Lopes CD, Pereira TA et al. In vitro and in vivo trypanocidal activity of H2bdtc-loaded solid lipid nanoparticles. PLoS Neglected Tropical Diseases 2014; 8 (5): e2847. doi: 10.1371/journal.pntd.0002847

8 Leigh M, Raines DJ, Castillo CE, Duhme-Klair AK. Inhibition of xanthine oxidase by thiosemicarbazones, hydrazones and dithiocarbazates derived from hydroxy-substituted benzaldehydes. ChemMedChem 2011; 6 (6): 1107-1118. doi: 10.1002/cmdc.201100054

9 Alafeefy AM, Kadi AA, Al-Deeb OA, El-Tahir KE, Al-jaber NA. Synthesis, analgesic and anti-inflammatory evaluation of some novel quinazoline derivatives. European Journal of Medicinal Chemistry 2010; 45 (11): 4947-4952. doi: 10.1016/j.ejmech.2010.07.067

10 Upmanyu N, Gupta JK, Shah K, Mishra P. Anti-inflammatory and antinociceptive evaluation of newly synthesized 4-(substituted ethanoyl) amino-3-mercapto-5-(4-methoxy) phenyl-1, 2, 4-triazoles. Journal of Pharmacy and Bioallied Sciences 2011; 3 (2): 259-265. doi: 10.4103/0975-7406.80783

11 Boschi A, Uccelli L, Duatti A, Colamussi P, Cittanti C et al. A kit formulation for the preparation of 188Re-lipiodol: preclinical studies and preliminary therapeutic evaluation in patients with unresectable hepatocellular carcinoma. Nuclear Medicine Communications 2004; 25 (7): 691-699. doi: 10.1097/01.mnm.0000130241.22068.45

12 Cerqueira NM, Fernandes PA, Ramos MJ. Ribonucleotide reductase: a critical enzyme for cancer chemotherapy and antiviral agents. Recent Patents on Anti-Cancer Drug Discovery 2007; 2 (1): 11-29. doi: 10.2174/157489207779561408

13 Chang F, Li PS, Huang Liu R, Hu HC, Hwang TL et al. Bioactive phenolic components from the twigs of Atalantia buxifolia. Journal of Natural Products 2018; 81 (7): 1534-1539. doi: 10.1021/acs.jnatprod.7b00938

14 Lasram S, Zemni H, Hamdi Z, Chenenaoui S, Houissa H et al. Antifungal and antiaflatoxinogenic activities of Carum carvi L., Coriandrum sativum L. seed essential oils and their major terpene component against Aspergillus flavus. Industrial Crops and Products 2019; 134 (1): 11-18. doi: 10.1016/j.indcrop.2019.03.037

15 Salminen A, Lehtonen M, Suuronen T, Kaarniranta K, Huuskonen j. Terpenoids: natural inhibitors of NF-κB signaling with anti-inflammatory and anticancer potential. Cellular and Molecular Life Sciences 2008; 65 (19): 2979-2999. doi: 10.1007/s00018-008-8103-5

16 Dinkova-Kostova A, Liby KT, Stephenson KK, Holtzclaw WD, Gao X et al. Extremely potent triterpenoid inducers of the phase 2 response: correlations of protection against oxidant and inflammatory stress. Proceedings of the National Academy of Sciences 2005; 102 (12): 4584-4589. doi: 10.1073/pnas.0500815102

17 Flechas MC, Ocazionez RE, Stashenko EE. Evaluation of in vitro antiviral activity of essential oil compounds against dengue virus. Pharmacognosy Journal 2018; 10 (1): 1-9. doi: 10.5530/pj.2018.1.11

18 Ali AM, Tarafdar M. Metal complexes of sulphur and nitrogen-containing ligands: complexes of s-benzyldithiocarbazate and a Schiff base formed by its condensation with pyridine-2-carboxaldehyde. Journal of Inorganic and Nuclear Chemistry 1977; 39 (10): 1785-1791. doi: 10.1016/0022-1902(77)80202-9

19 Otwinowski Z, Minor W. Processing of X-ray diffraction data collected in oscillation mode. Methods in Enzymology 1997; 276: 307-326. doi: 10.1016/S0076-6879(97)76066-X

20 Sheldrick GM. SHELXT–Integrated space-group and crystal-structure determination. Acta Crystallographica Section A: Foundations and Advances 2015; 71 (1): 3-8. doi: 10.1107/S2053273314026370

21 Dolomanov OV, Bourhis LJ, Gildea RJ, Howard JA, Puschmann H. OLEX2: a complete structure solution, refinement and analysis program. Puschmann, Journal of Applied Crystallography 2009; 42 (2): 339-341. doi: 10.1107/S0021889808042726

22 Farrugia, LJ. WinGX and ORTEP for Windows: an update. Journal of Applied Crystallography 2012; 45 (4): 849-854. doi: 10.1107/S0021889812029111

23 Brandenburg K, Putz H. DIAMOND - Crystal and Molecular Structure Visualization - Demonstration Version 3.2k. Bonn, Germany: Crystal Impact GbR, 2006.

24 Spek AL. Structure validation in chemical crystallography. Acta Crystallographica Section D: Biological Crystallography 2009; 65 (2): 148-155. doi: 10.1107/S090744490804362X

25 Lindenbach BD. Measuring HCV infectivity produced in cell culture and in vivo Hepatitis C. Springer 2009; (1): 329-336. doi: 10.1007/978-1-59745-394-3_24

26 Zandi K, Lim TH, Rahim NA, Shu MH, Teoh BT et al. Extract of Scutellaria baicalensis inhibits dengue virus replication. BMC Complementary and Alternative Medicine 2013; 13 (1): 91. doi: 10.1186/1472-6882-13-91

27 Tang LI, Ling AP, Koh RY, Chye SM, Voon KG. Screening of anti-dengue activity in methanolic extracts of medicinal plants. BMC Complementary and Alternative Medicine 2012; 12 (1): 3. doi: 10.1186/1472-6882-12-3

28 Kudi A, Myint S. Antiviral activity of some Nigerian medicinal plant extracts. Journal of Ethnopharmacology 1999; 68 (1-3): 289-294. doi: 10.1016/s0378-8741(99)00049-5

29 Keivan Z, Boon-Teong T, Sing-Sin S, Pooi-Fong W, Mustafa MR et al. In vitro antiviral activity of fisetin, rutin and naringenin against dengue virus type-2. Journal of Medicinal Plants Research 2011; 5 (23): 5534-5539. doi: 10.5897/JMPR11.1046

30 Bhat RA, Kumar D, Alam A, Mir BA, Srivastava A et al. Synthesis, characterization, thermal and DFT studies of S-methyl-β-N-(3-(2-nitrophenyl) allylidene dithiocarbazate as anti-bacterial agent. Journal of Molecular Structure 2018; 1173 (1): 72-80. doi: 10.1016/j.molstruc.2018.06.061

31 Crouse KA, Chew KB, Tarafder M, Kasbollah A, Ali A et al. Synthesis, characterization and bio-activity of S-2-picolyldithiocarbazate (S2PDTC), some of its Schiff bases and their Ni (II) complexes and X-ray structure of S-2-picolyl-β-N-(2-acetylpyrrole) dithiocarbazate. Polyhedron 2004; 23 (1): 161-168. doi: 10.1016/j.poly.2003.09.025

32 Ali MA, Mirza AH, Butcher RJ, Crouse KA. The preparation, characterization and biological activity of palladium (II) and platinum (II) complexes of tridentate NNS ligands derived from S-methyl-and S-benzyldithiocarbazates and the X-ray crystal structure of the [Pd (mpasme) Cl] complex. Transition Metal Chemistry 2006; 31 (1): 79-87. doi: 10.1007/s11243-005-6305-3

33 Takjoo R, Centore R, Rhyman L, Ramasami P. Nickel (II) and copper (II) complexes of allyl 2-(thiophen-2-ylmethylene) hydrazinecarbodithioate: synthesis, X-ray crystal structures, and theoretical study. Journal of Coordination Chemistry 2012, 65 (9): 1569-1579. doi: 10.1080/00958972.2012.675058

34 Peracchi A, Bettati S, Mozzarelli A, Rossi GL, Miles EW et al. Allosteric regulation of tryptophan synthase: effects of pH, temperature, and α-subunit ligands on the equilibrium distribution of pyridoxal 5 '-phosphate– l-serine intermediates. Biochemistry 1996; 35 (6): 1872-1880. doi: 10.1021/bi951889c

35 Grooms CR, Bruno IJ, Lightfoot MP, Ward SC. The Cambridge structural database. Acta Crystallographica Section B: Structural Science, Crystal Engineering and Materials 2016; 72 (2): 171-179. doi: 10.1107/S2052520616003954

36 Mundlapati VR, Gautam S, Sahoo DK, Ghosh A, Biswal HS. Thioamide, a hydrogen bond acceptor in proteins and nucleic acids. The Journal of Physical Chemistry Letters 2017; 8 (18): 4573-4579. doi: 10.1021/acs.jpclett.7b01810

37 McConathy J, Owens MJ. Stereochemistry in drug action. Primary Care Companion to the Journal of Clinical Psychiatry 2003; 5 (2): 70-73. doi: 10.4088/pcc.v05n0202

38 Low ML, Maigre L, Dorlet P, Guillot R, Pagès JM et al. Conjugation of a new series of dithiocarbazate Schiff base copper (II) complexes with vectors selected to enhance antibacterial activity. Bioconjugate Chemistry 2014; 25 (12): 2269-2284. doi: 10.1021/bc5004907

39 Leandro LM, De Sousa VF, Barbosa PS, Neves KO, Da Silva JA et al. Chemistry and biological activities of terpenoids from copaiba (Copaifera spp.) oleoresins. Molecules 2012; 17 (4): 3866-3889. doi: 10.3390/molecules17043866

40 Bakkali F, Averbeck S, Averbeck D, Idaomar M. Biological effects of essential oils –a review. Food and Chemical Toxicology 2008; 46 (2): 446-475. doi: 10.1016/j.fct.2007.09.106

41 Culley S, Towers G, Selwood D, Henriques R, Grove J. Infection counter: automated quantification of in vitro virus replication by fluorescence microscopy. Viruses 2016; 8 (7): 201. doi: 10.3390/v8070201

Supplementary Materials

Synthesis and anti-dengue evaluation of enantiomeric S-substituted dithiocarbazates-derived Schiff bases

Maqsood MARYAM[1, 2], Sang Loon TAN[3,4] , Mohamed Ibrahim MOHAMED TAHIR,.[3*], Hui-Yee CHEE[2*]

[1] Faculty of Natural Sciences, SBKW University Balochistan, 83300 Quetta, Pakistan

[2] Department of Medical Microbiology and Parasitology, Faculty of Medicine and Health Sciences, Universiti Putra Malaysia, 43400 UPM Serdang, Selangor, Malaysia

[3] Department of Chemistry, Faculty of Science, Universiti Putra Malaysia, 43400 UPM Serdang, Selangor, Malaysia

[4] Research Centre for Crystalline Materials, School of Science and Technology, Sunway University, 47500 Bandar Sunway, Selangor, Malaysia (current address)

Table of Contents

		The percentages of foci reduction were obtained by comparing against untreated cells maintained in parallel. The dose-response curve was plotted and IC50 dose was calculated using Graph Pad Prism Version 5 (Graph Pad Software Inc., San Diego, CA.).	

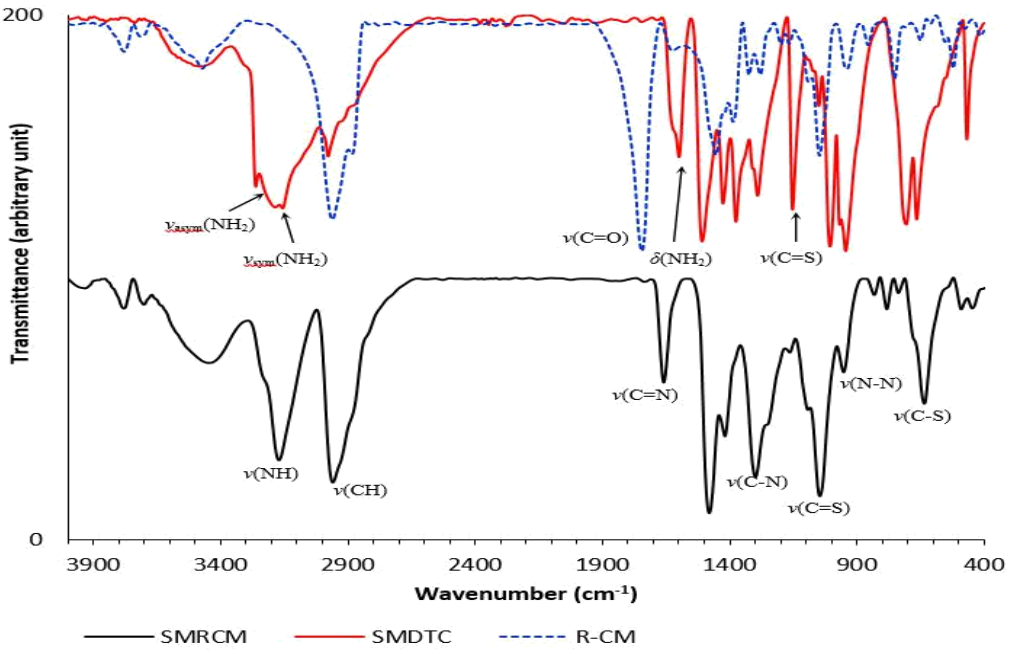

Figure S1: Comparison of IR spectra between SMRCM and its precursors

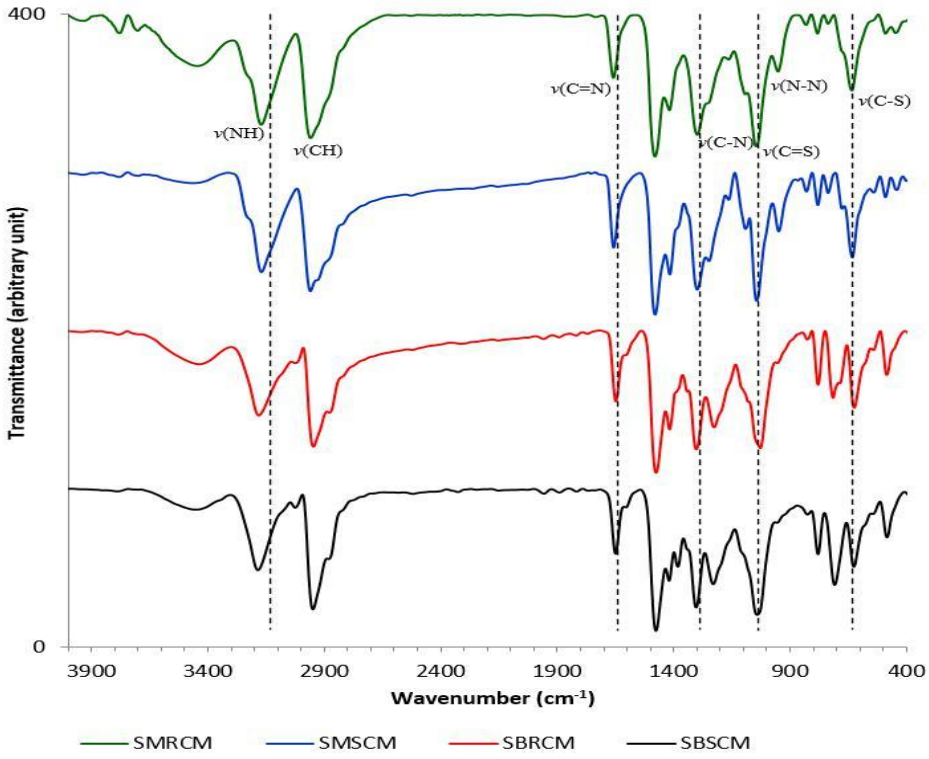

Figure S2: Comparison of IR spectra between SMRCM, SMSCM, SBRCM and SBSCM.

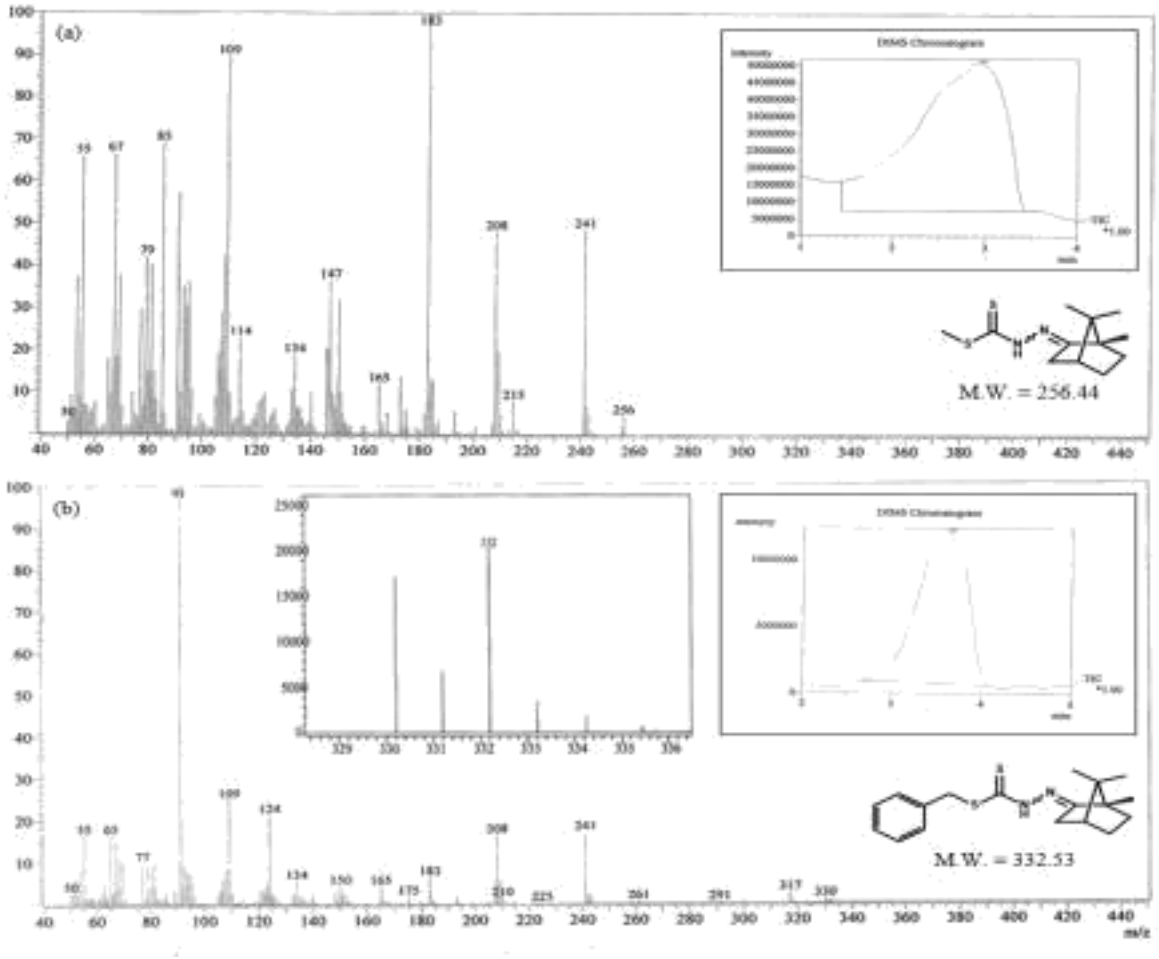

Figure S4: EI-MS spectra of (a) SMRCM, and (b) SBRCM. The spectra of SMSCM and SBSCM are identical to the (*R*)-enantiomers, respectively.

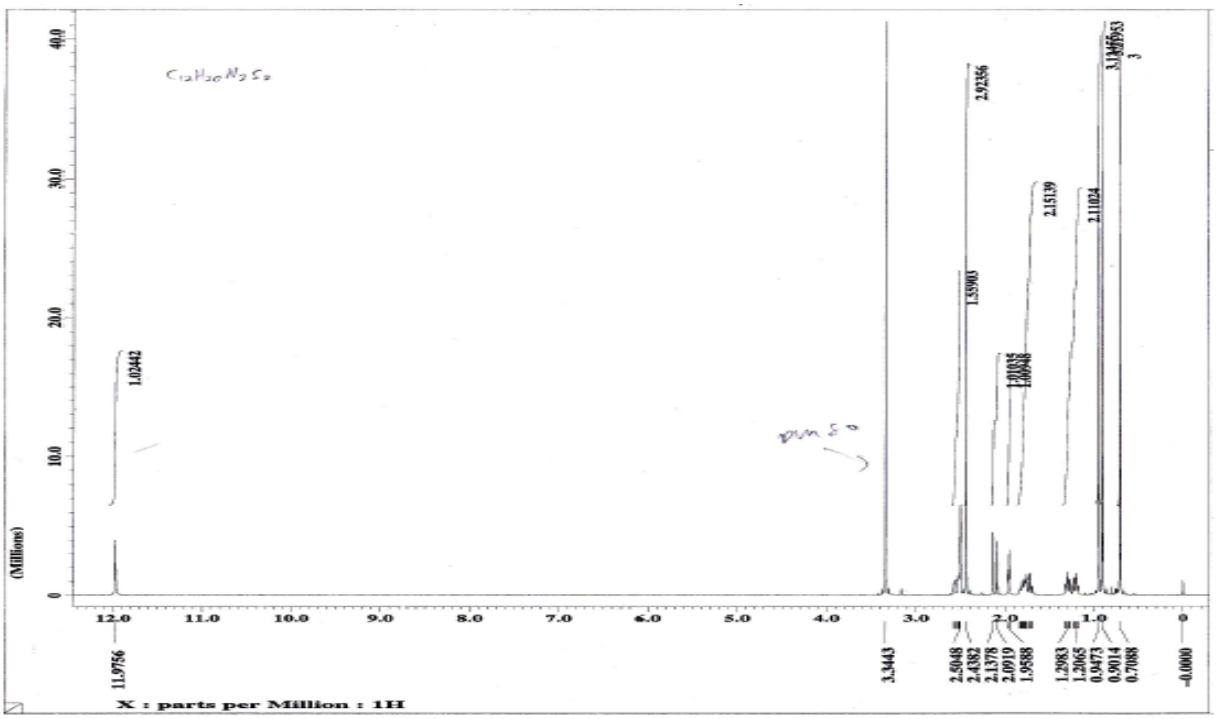

Figure S4: ^{1}H NMR Spectrum for SMRCM

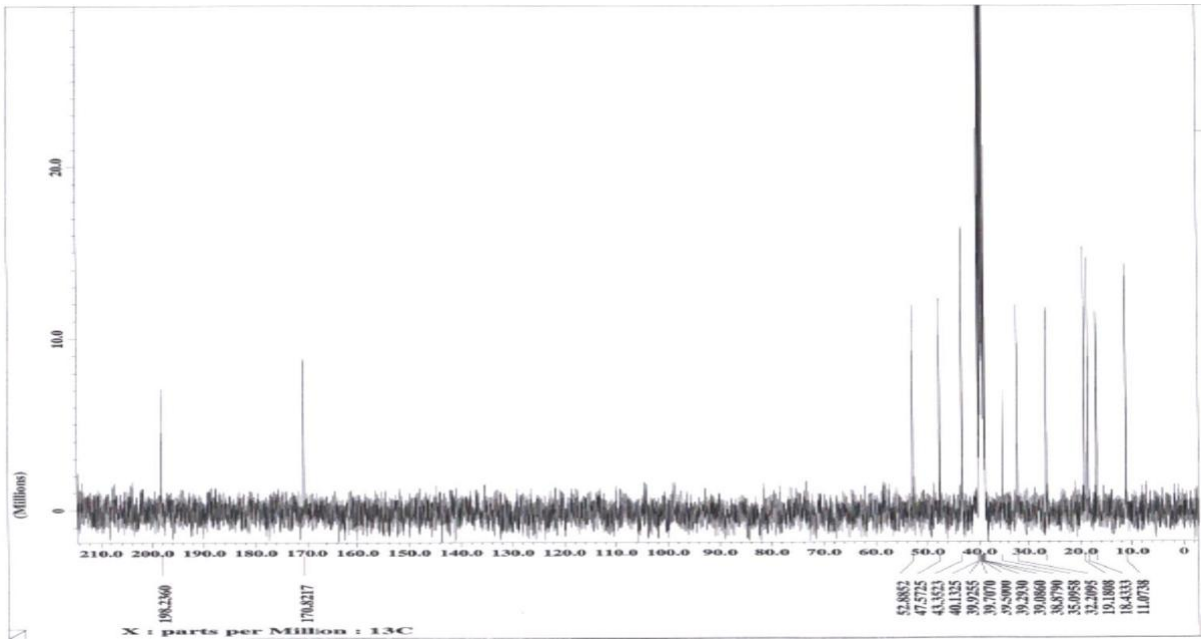

Figure S5: ^{13}C{^{1}H} NMR Spectrum for SMRCM

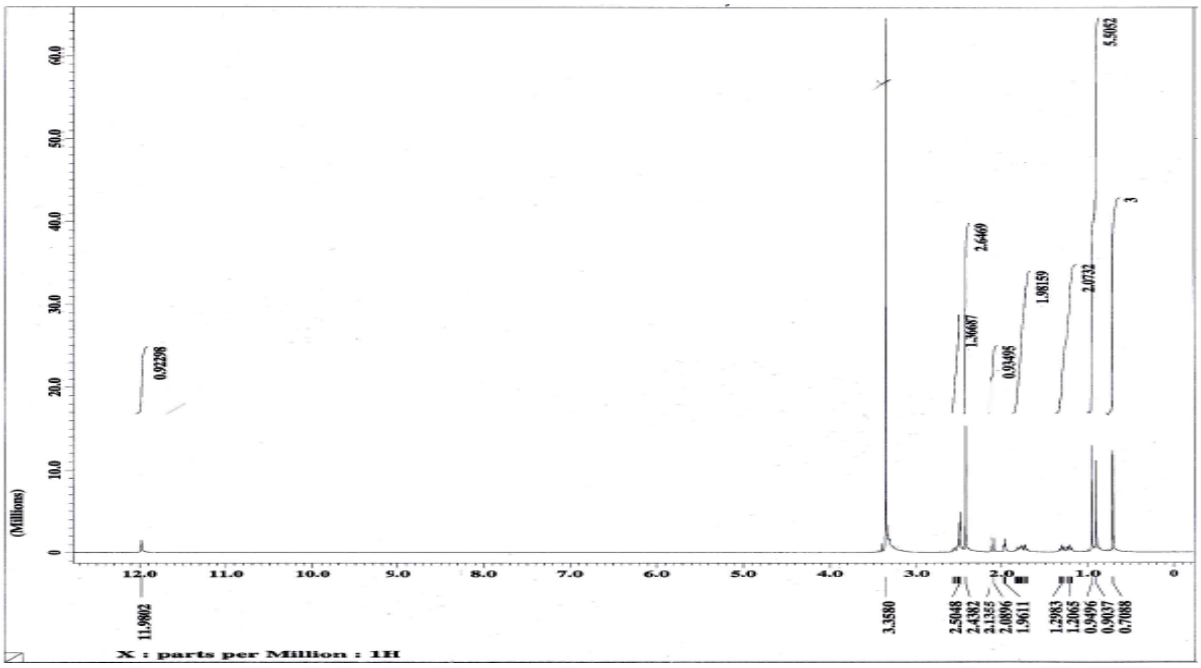

Figure S6: ^{1}H NMR Spectrum for SMSCM

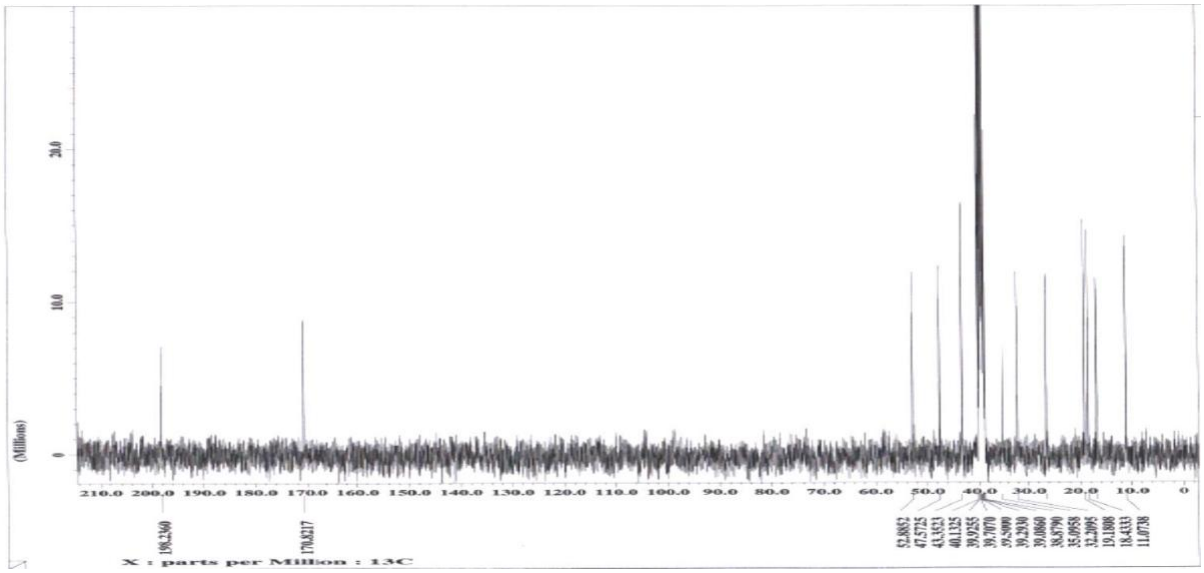

Figure S7: ^{13}C{^{1}H} NMR Spectrum for SMSCM

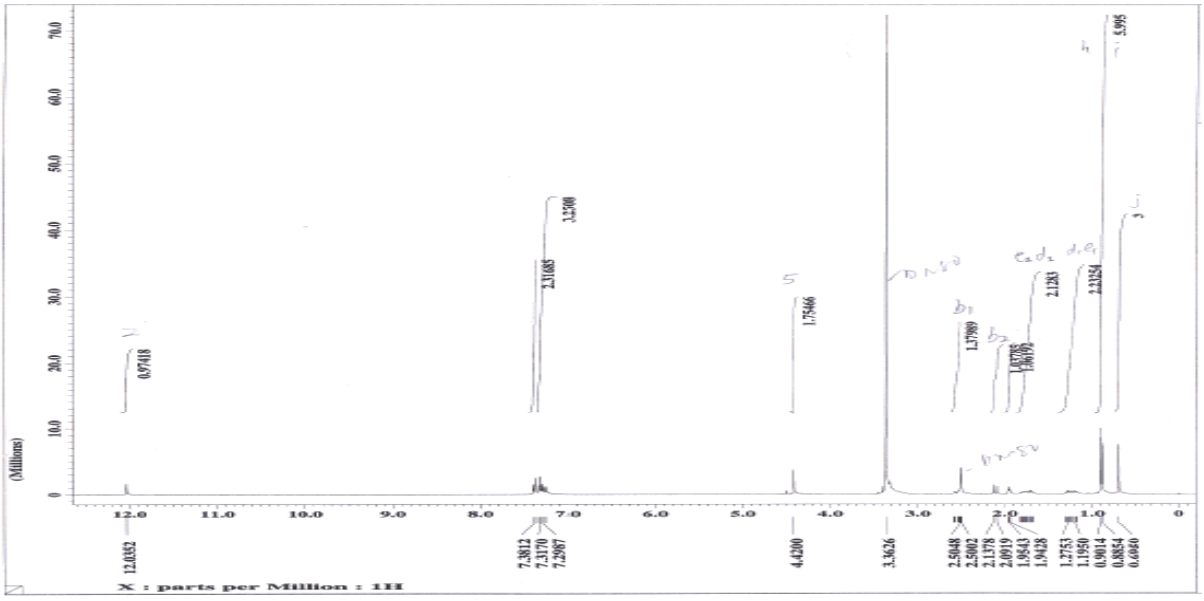

Figure S8: ^{1}H NMR Spectrum for SBRCM

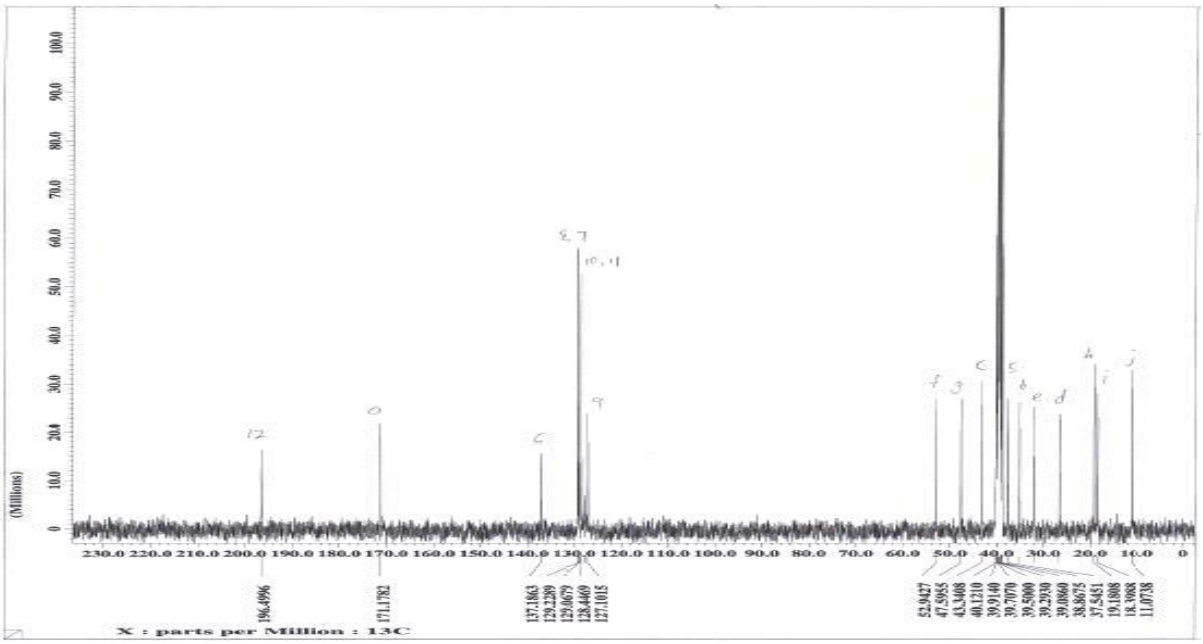

Figure S9: ^{13}C{^{1}H} NMR Spectrum for SBRCM

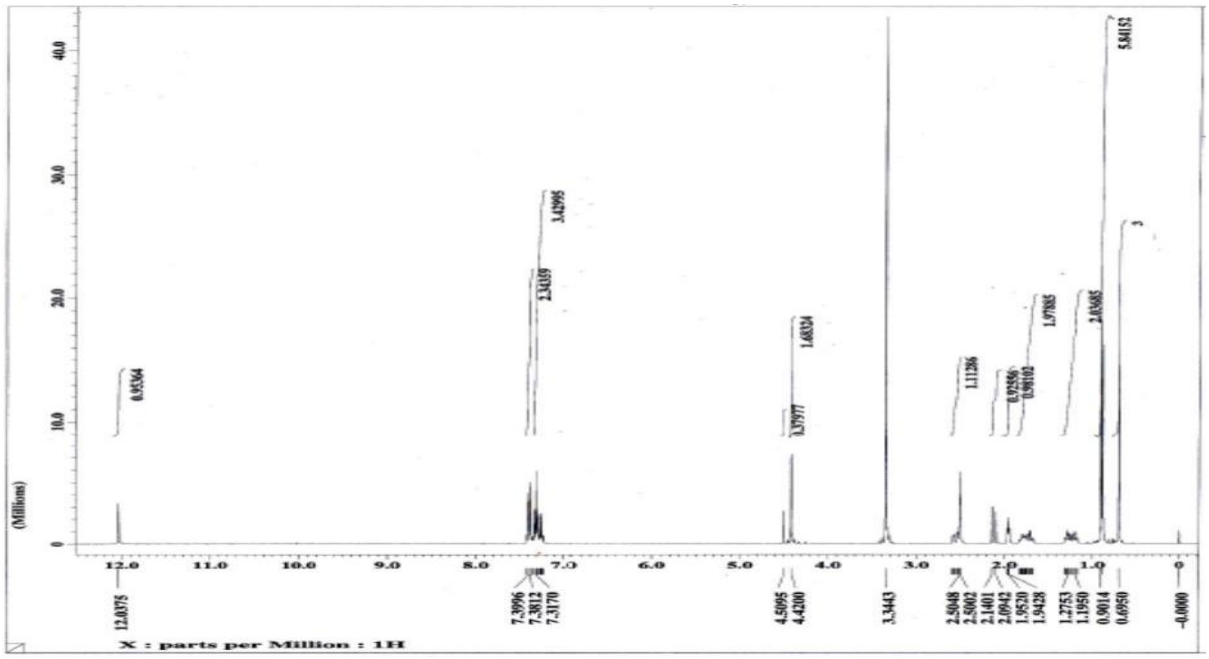

Figure S10: ^{1}H NMR Spectrum for SBSCM

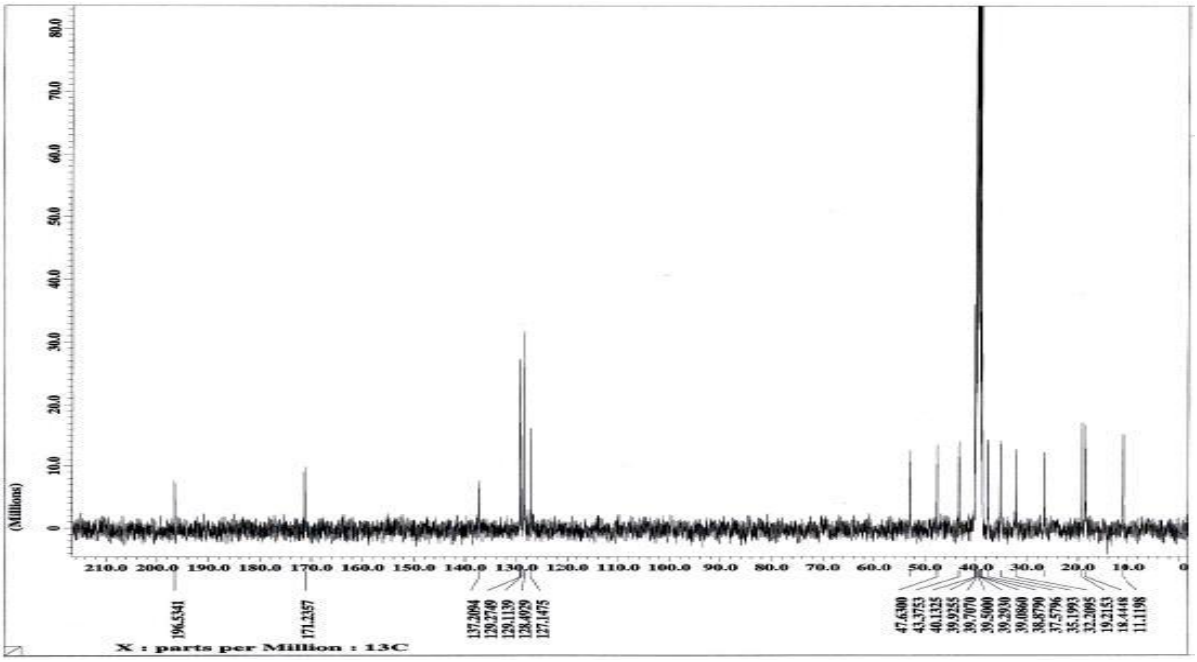

Figure S11: ^{13}C{^{1}H} NMR Spectrum for SBSCM

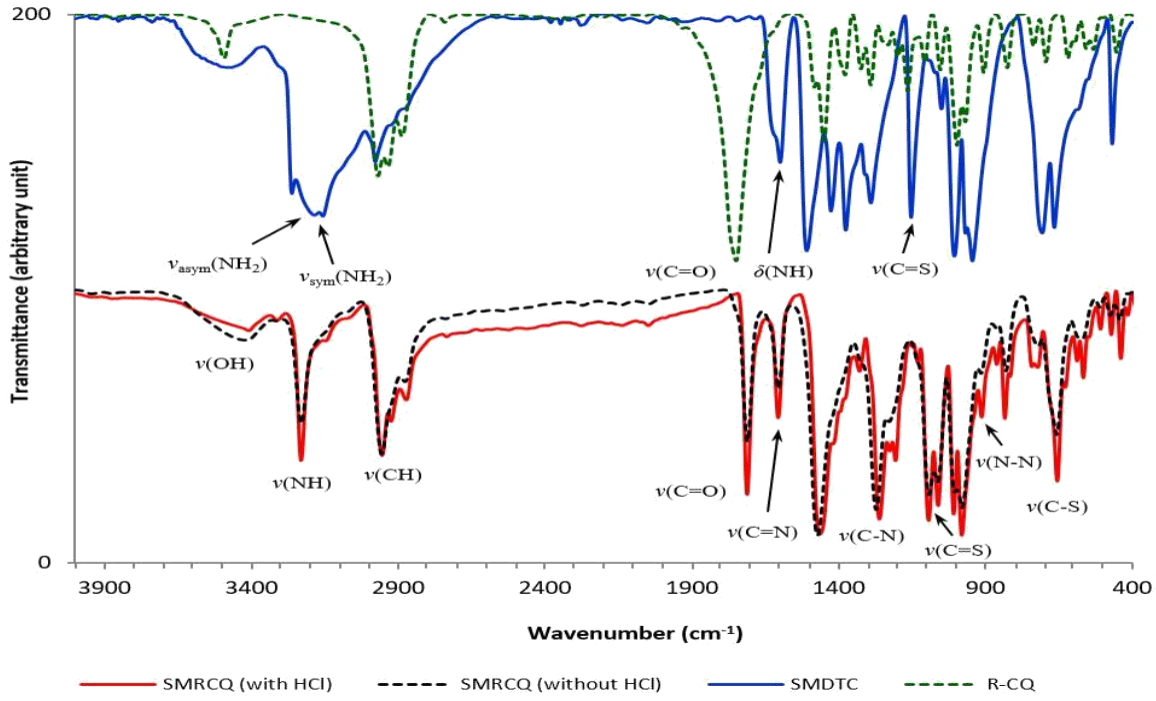

Figure S12: Comparison of IR spectra between SMRCQ and its precursors.

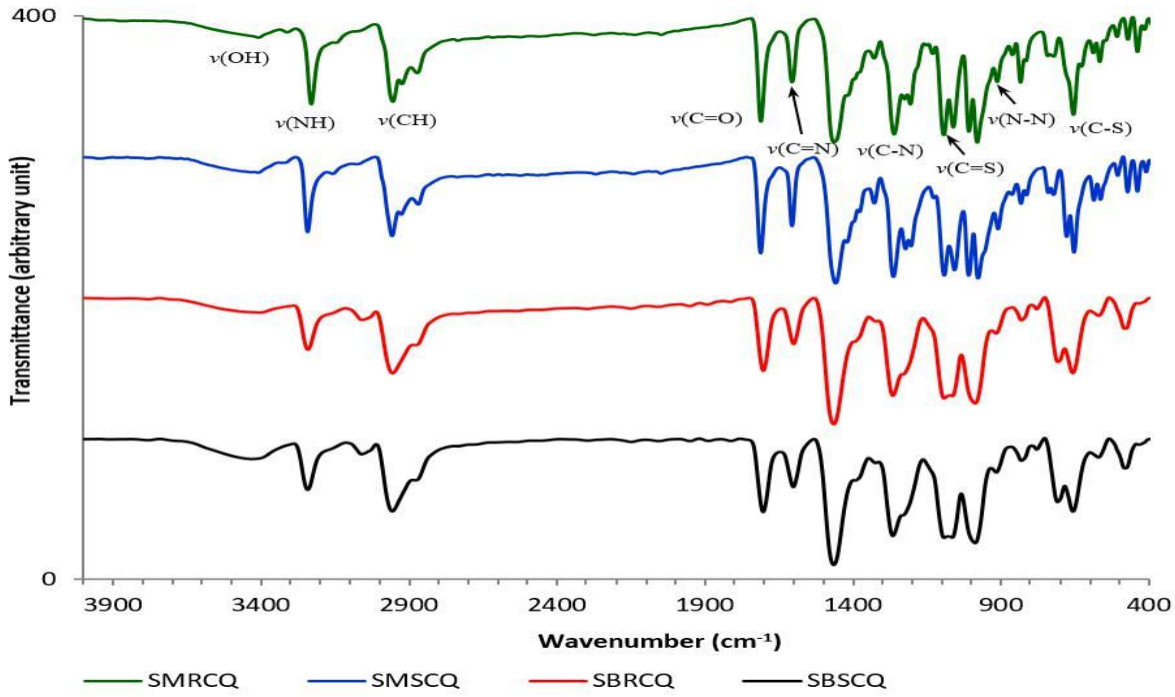

Figure S13: Comparison of IR spectra between SMRCQ, SMSCQ, SBRCQ and SBSCQ.

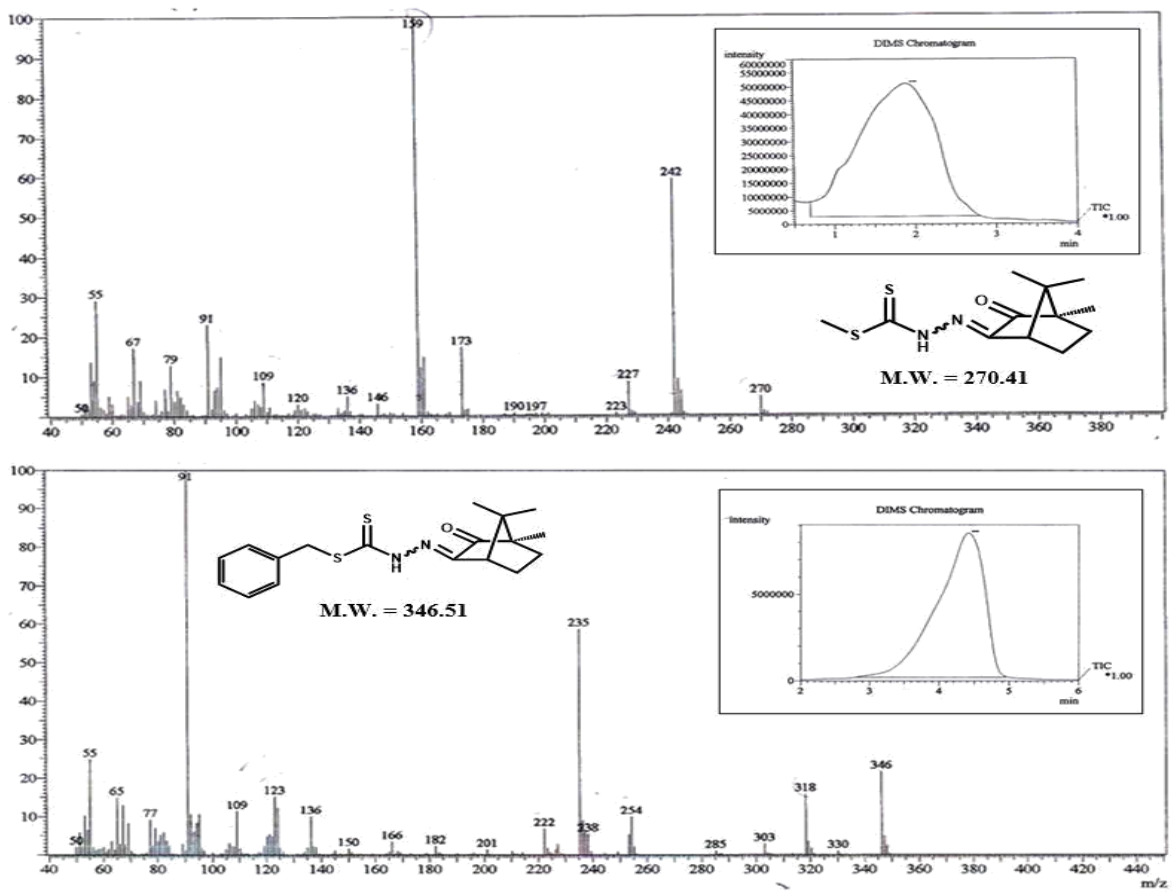

Figure S14: EI-MS spectra of SMRCQ (top) and SBRCQ (bottom). The spectra of SMSCQ and SBSCQ are identical to the (*R*)-enantiomers.

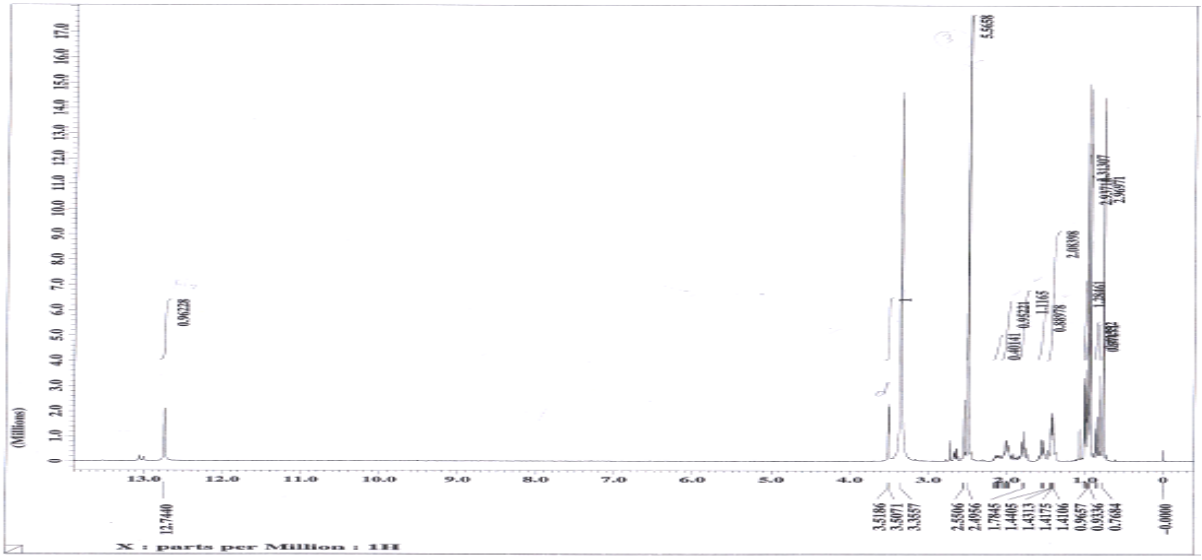

Figure S15: ^{1}H NMR Spectrum for SMRCQ

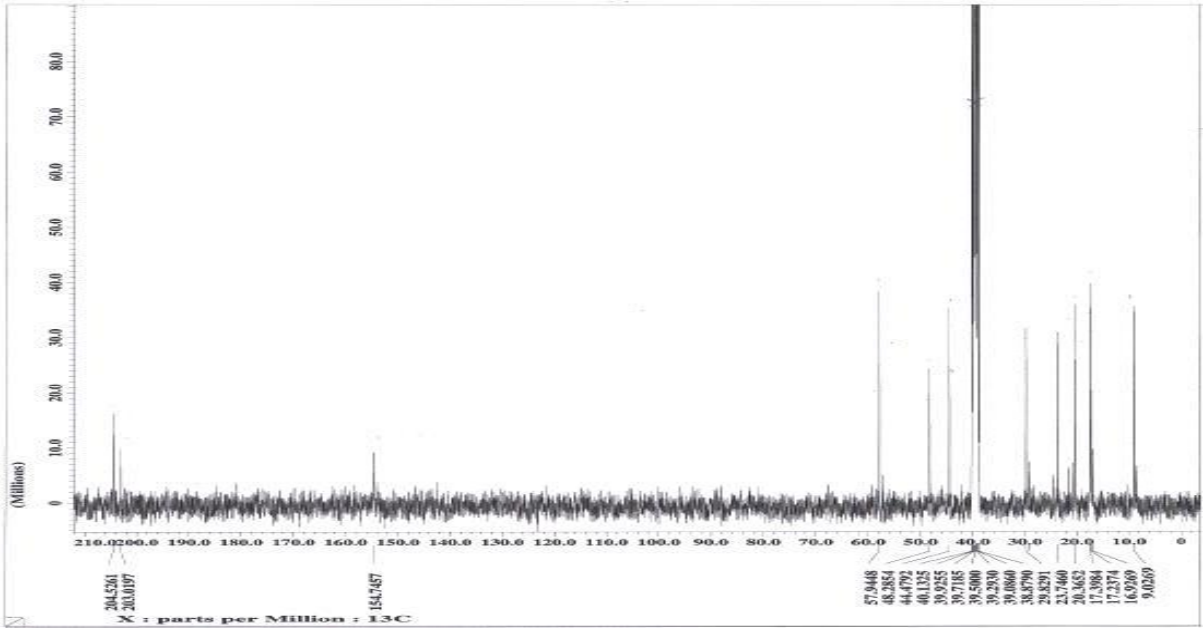

Figure S16: ^{13}C{^{1}H} NMR Spectrum for SMRCQ

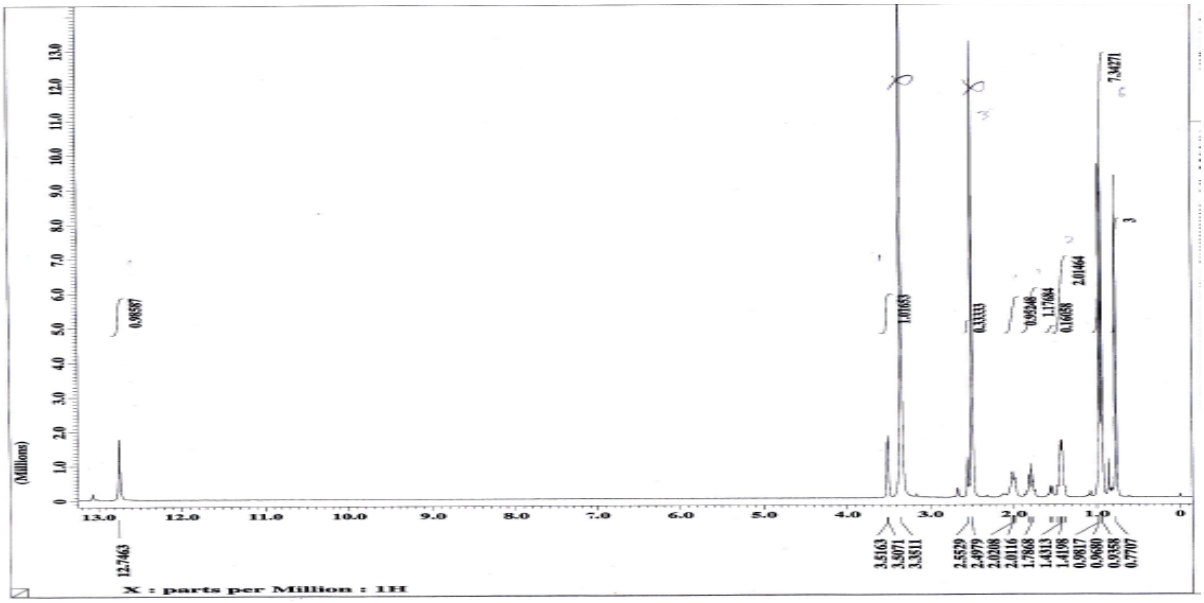

Figure S17: ^{1}H NMR Spectrum for SMSCQ

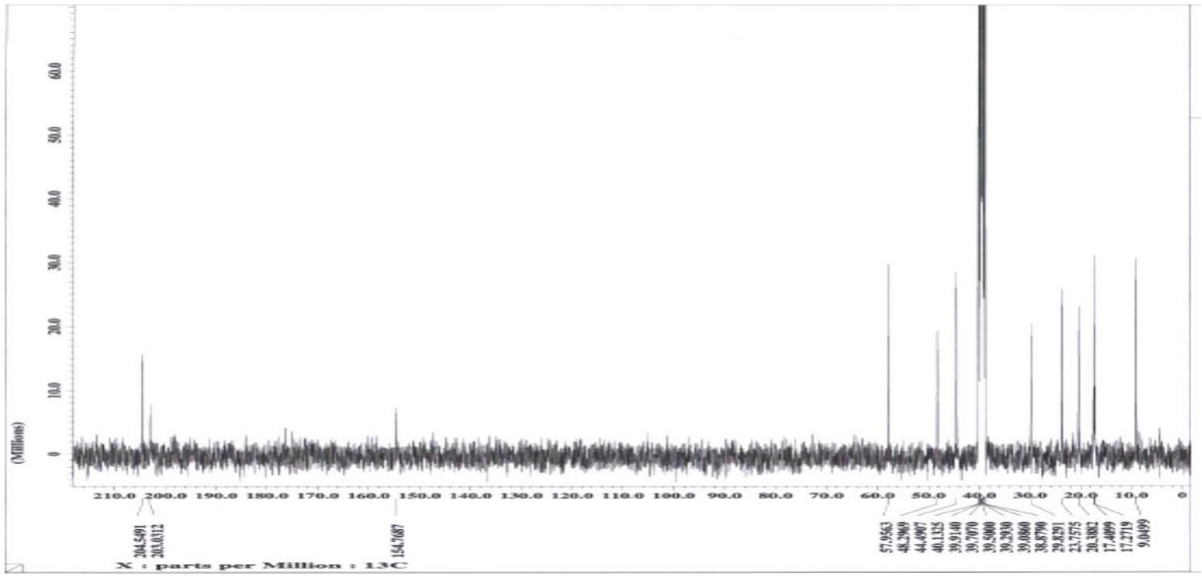

Figure S18: $^{13}C\{^{1}H\}$ NMR Spectrum for SMSCQ

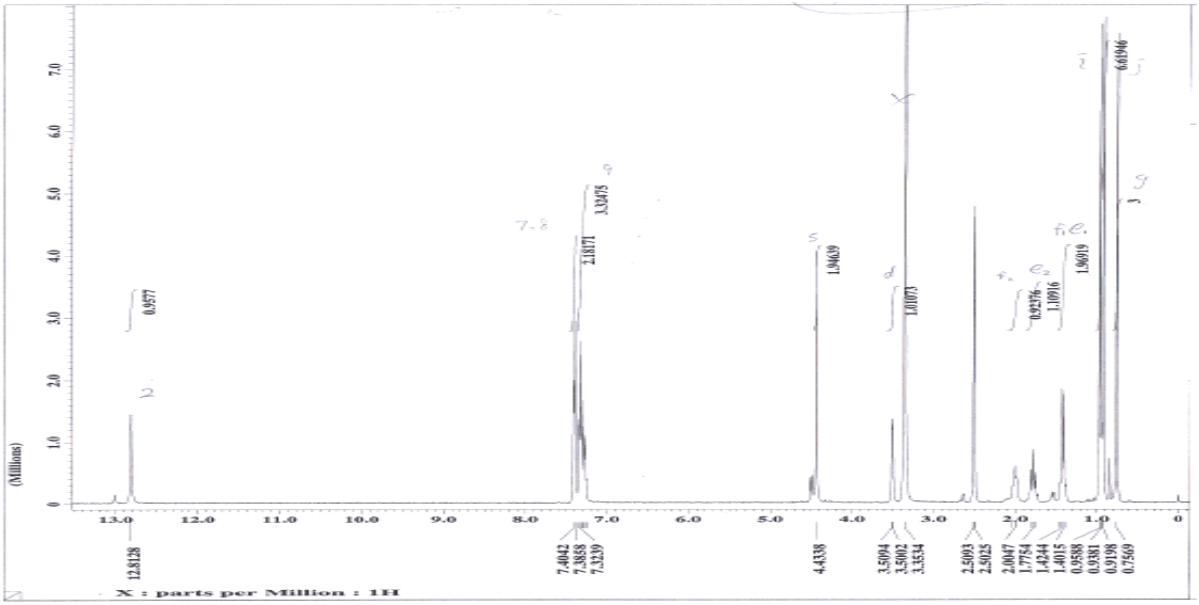

Figure S19: ^{1}H NMR Spectrum for SBRCQ

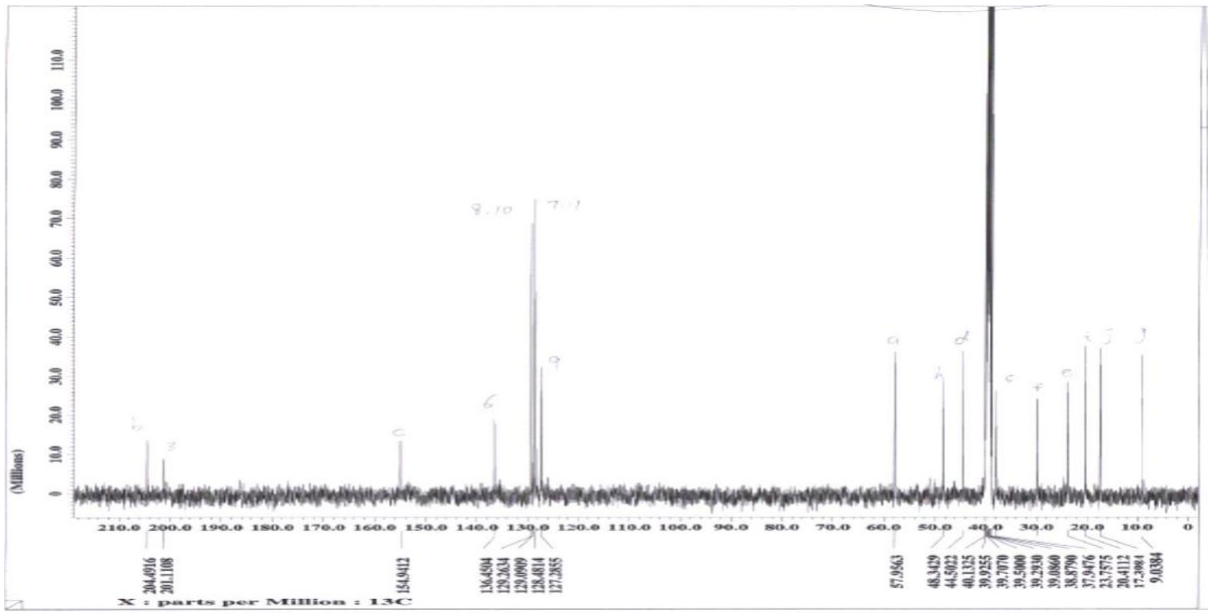

Figure S20: ^{13}C{^{1}H} NMR Spectrum for SBRCQ

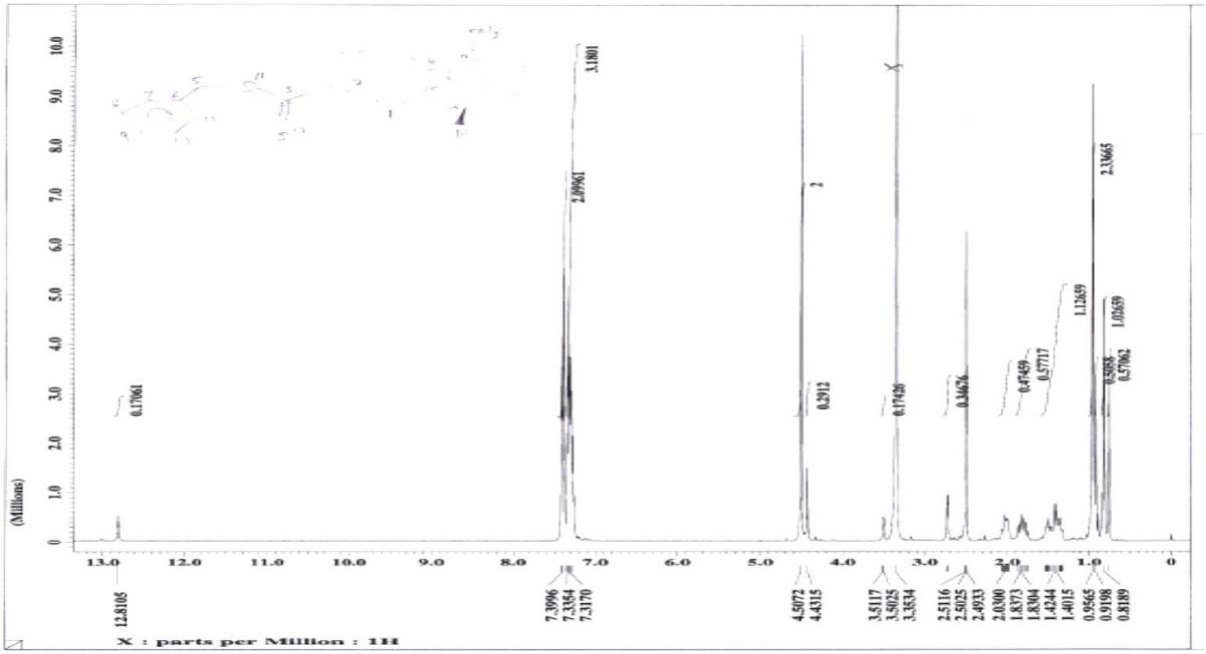

Figure S21: ^{1}H NMR Spectrum for SBSCQ

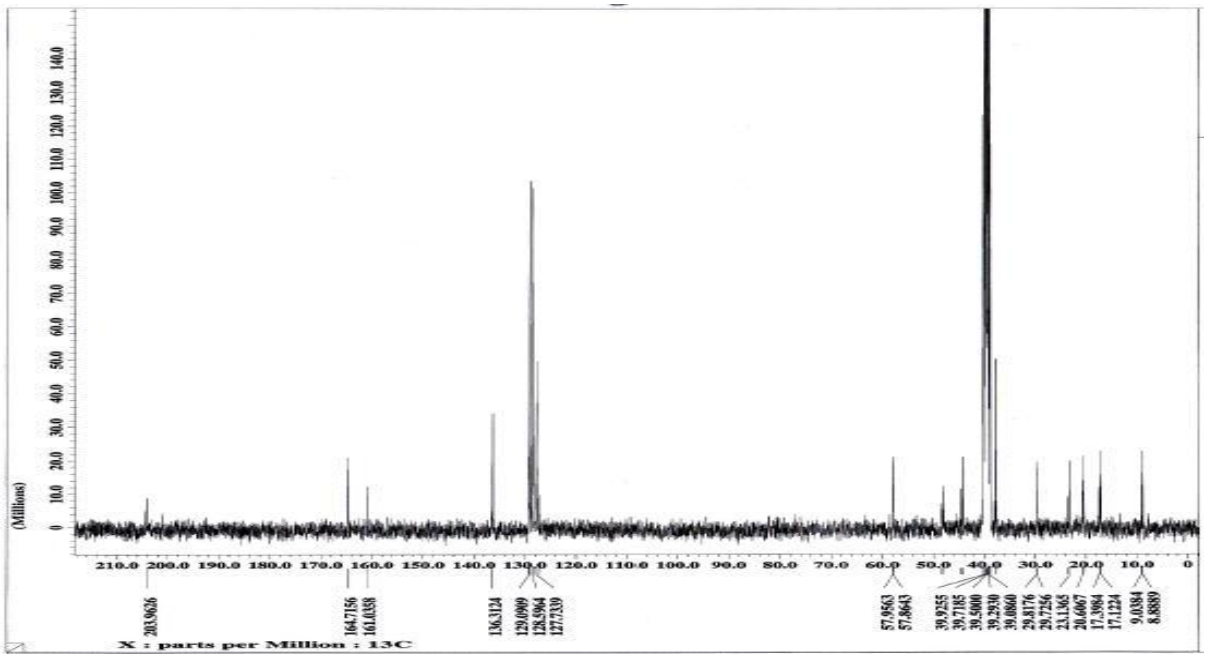

Figure S22: ^{13}C{^{1}H} NMR Spectrum for SBSCQ

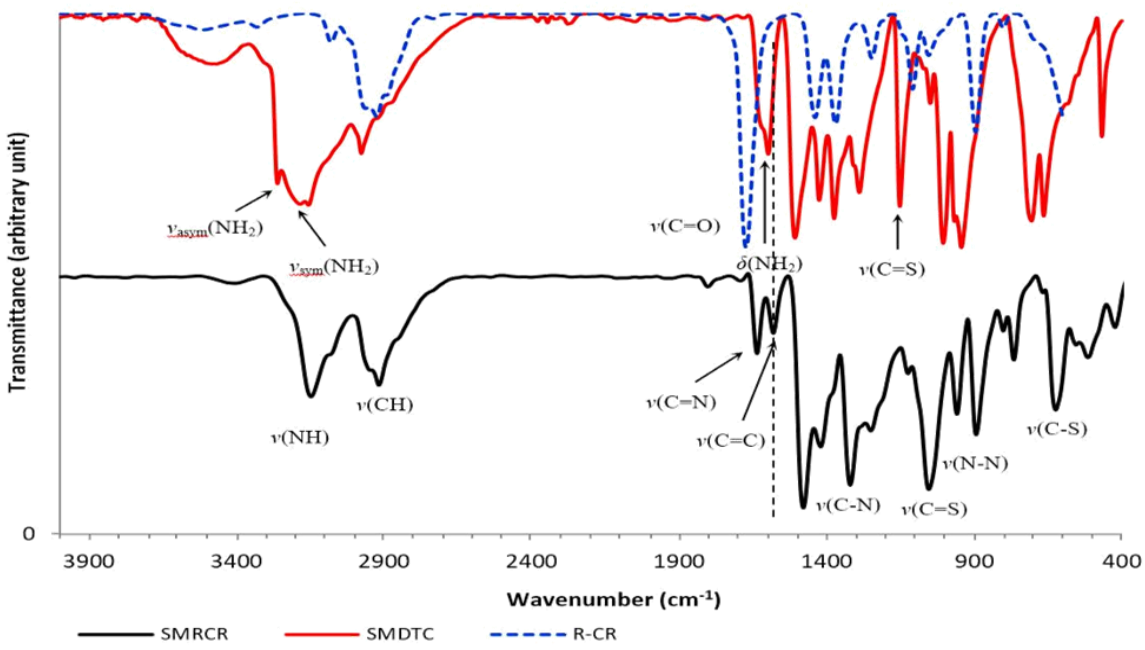

Figure S23: Comparison of IR spectra between SMRCV and its precursors.

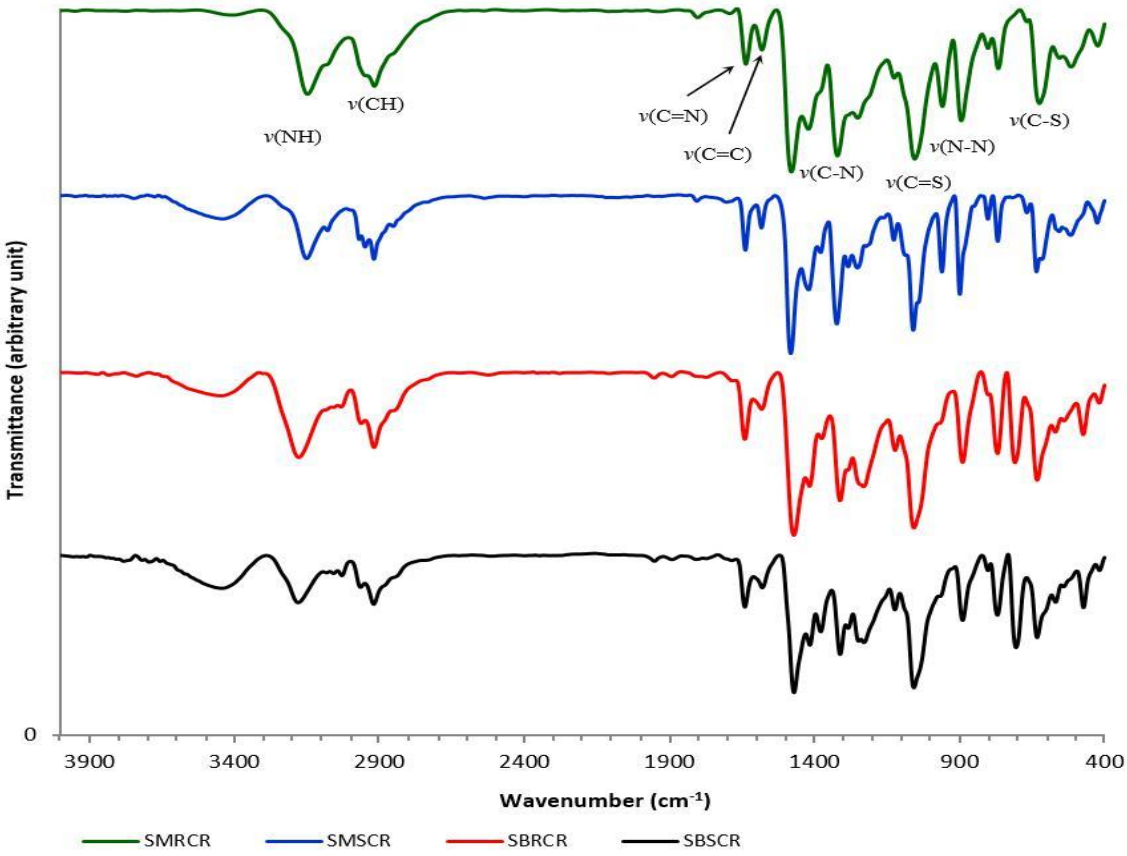

Figure S24: Comparison of IR spectra between SMRCV, SMSCV, SBRCV and SBSCV.

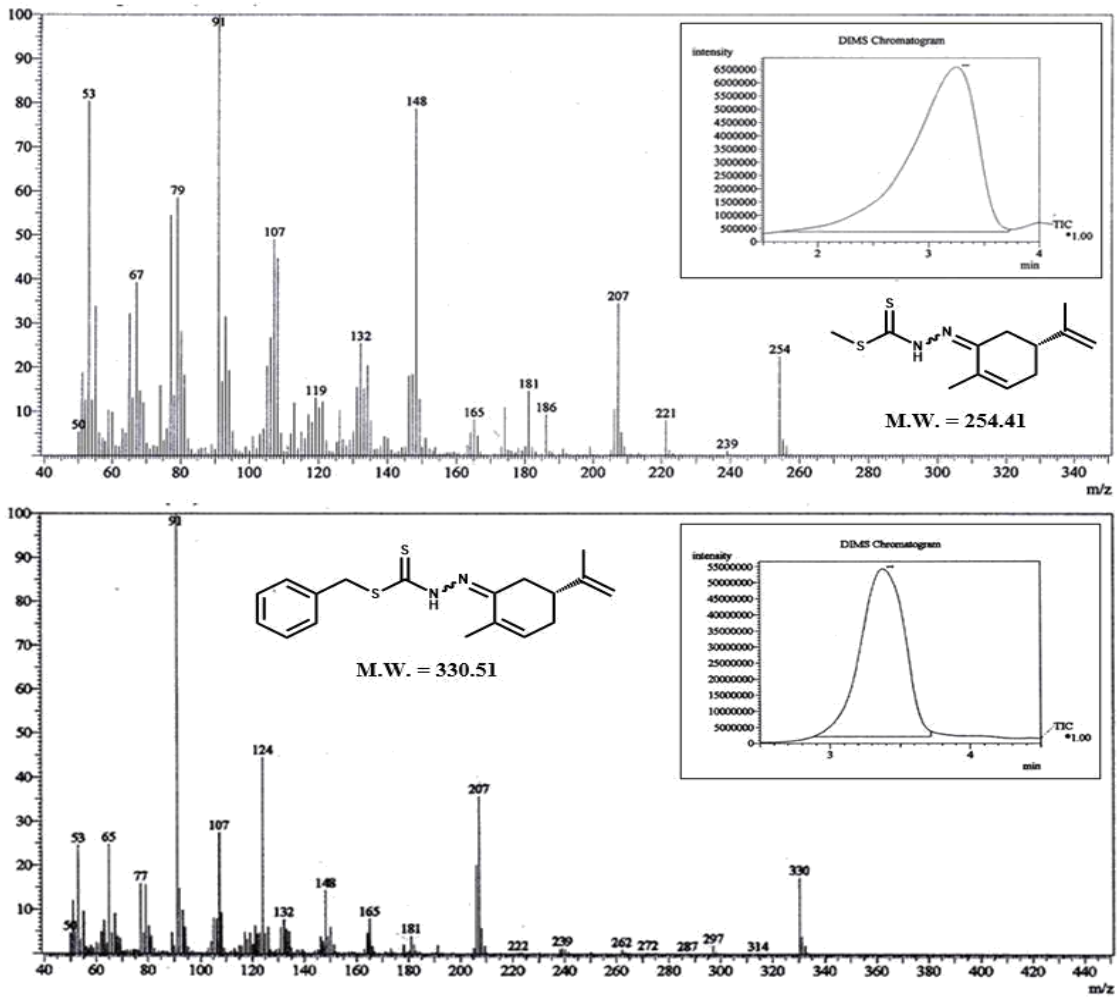

Figure S25: EI-MS spectra of SMRCV (top) and SBRCV (bottom). The spectra of SMSCV and SBSCV are identical to the (*R*)-enantiomers.

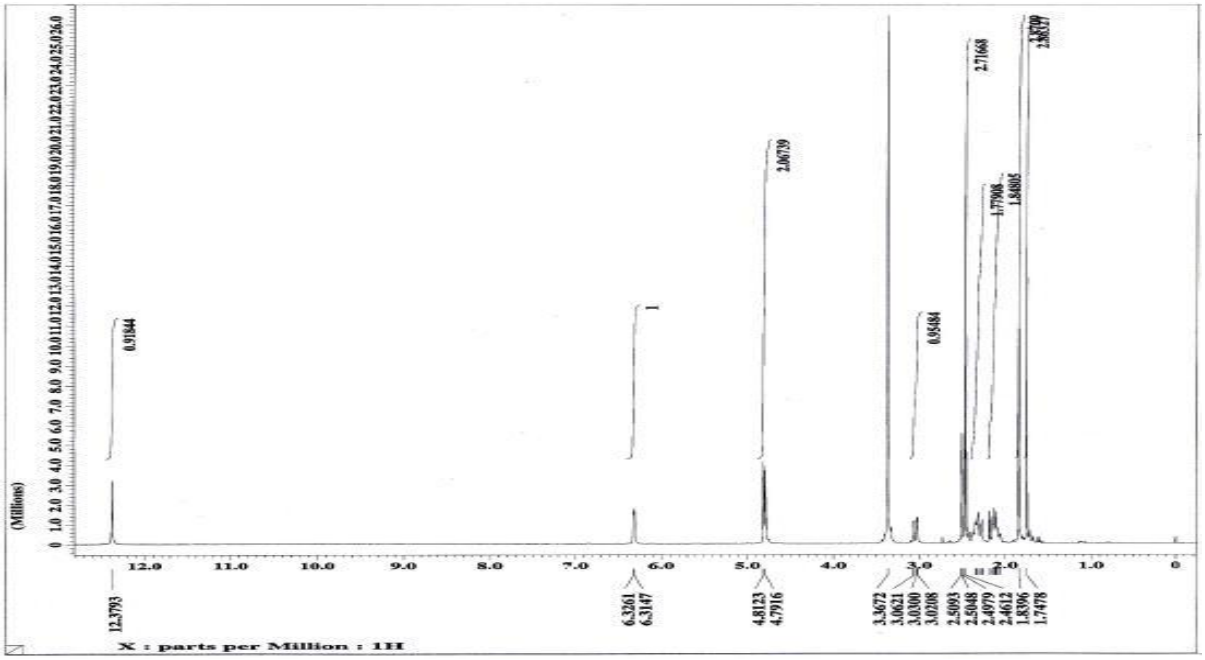

Figure S26: ^{1}H NMR Spectrum for SMRCV

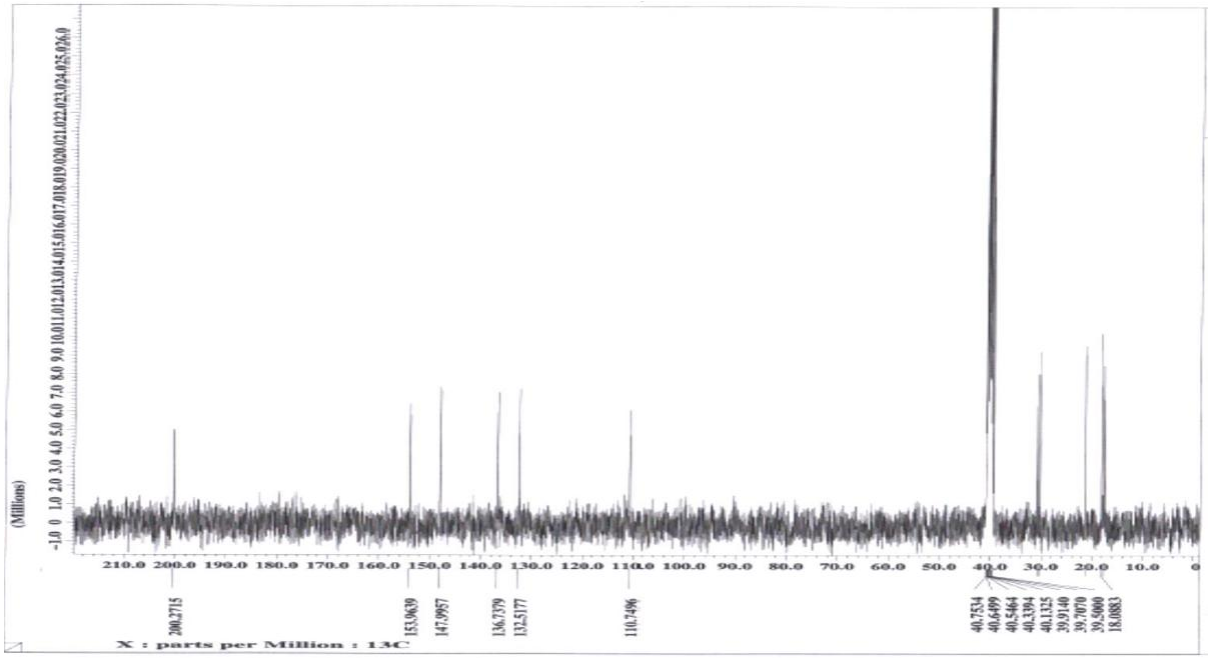

Figure S27: ^{13}C{^{1}H} NMR Spectrum for SMRCV

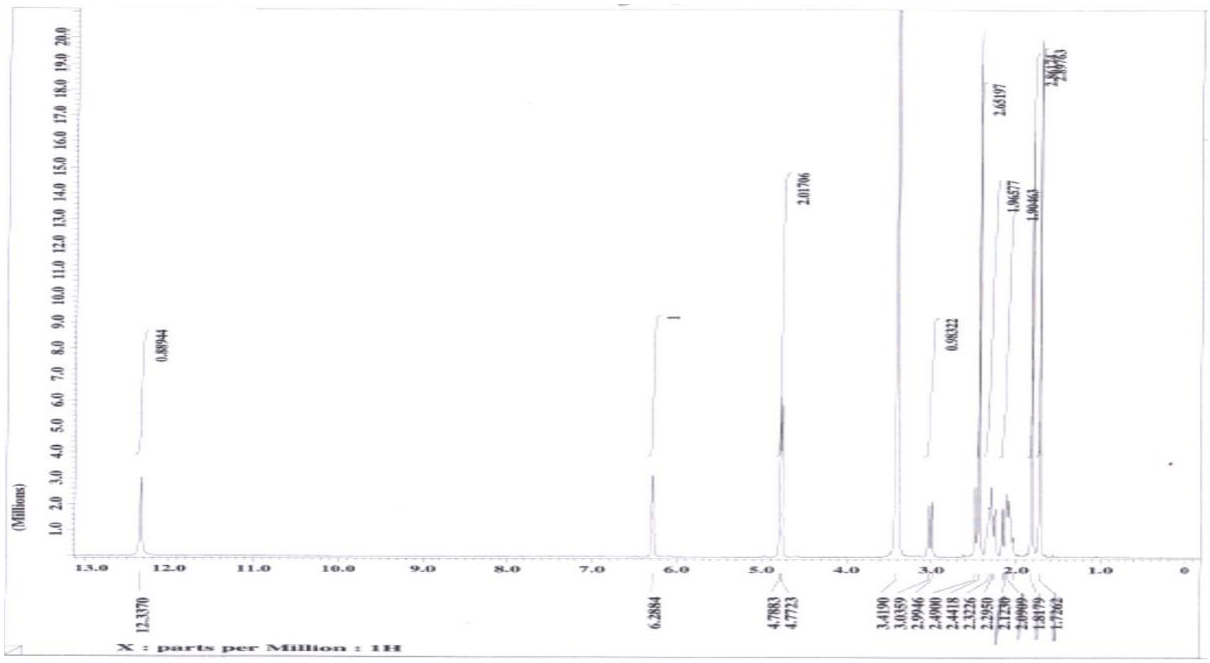

Figure S28: ^{1}H NMR Spectrum for SMSCV

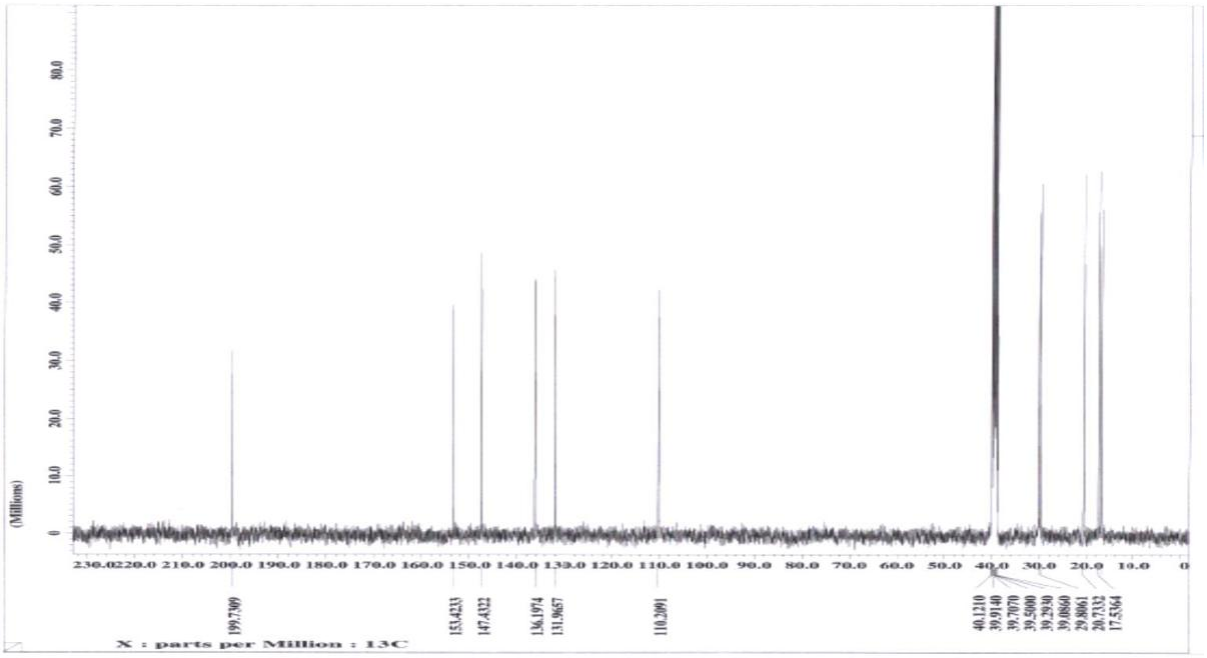

Figure S29: ^{13}C{^{1}H} NMR Spectrum for SMSCV

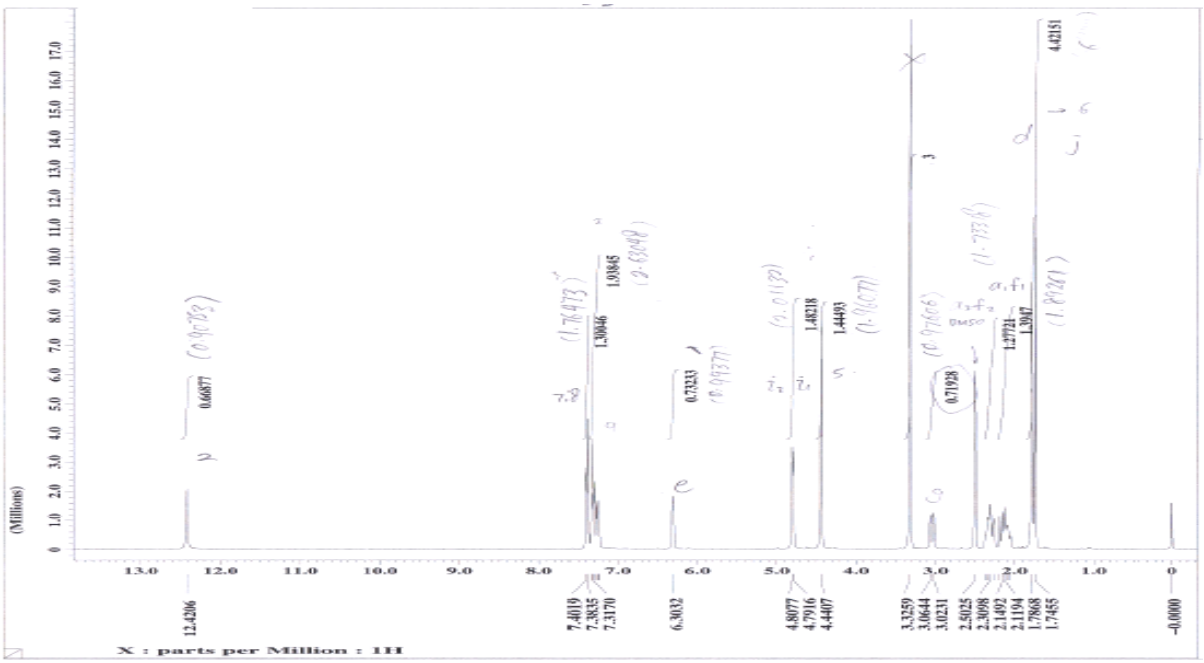

Figure S30: ^{1}H NMR Spectrum for SBRCV

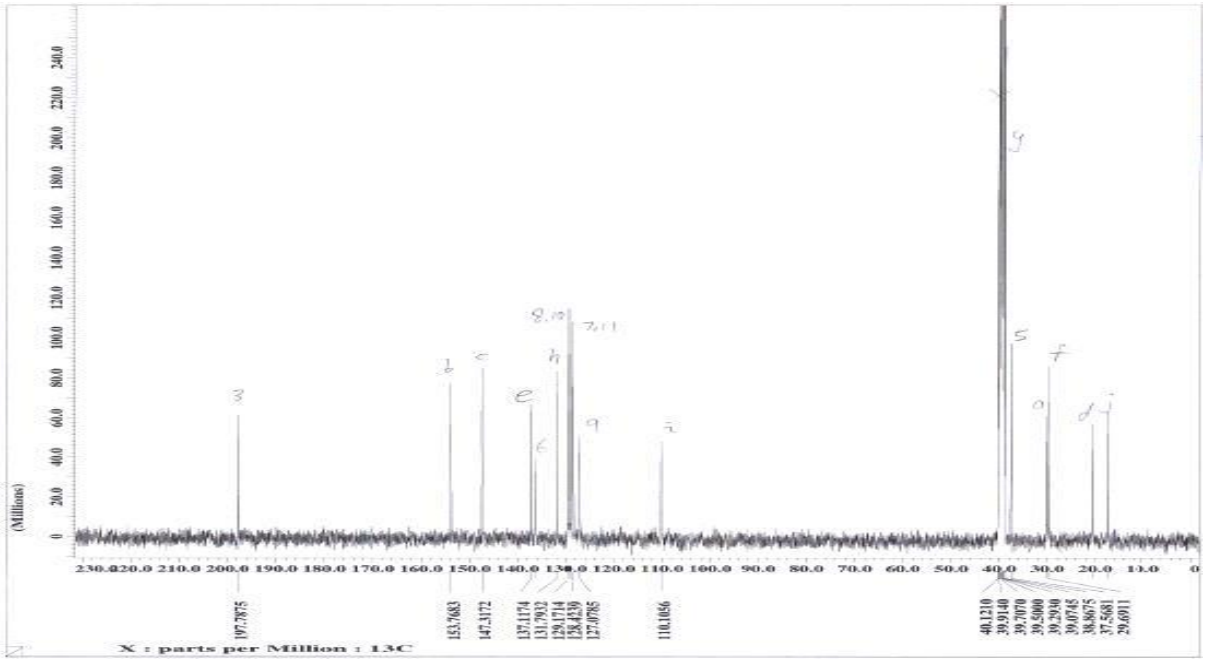

Figure S31: ^{13}C{^{1}H} NMR Spectrum for SBRCV

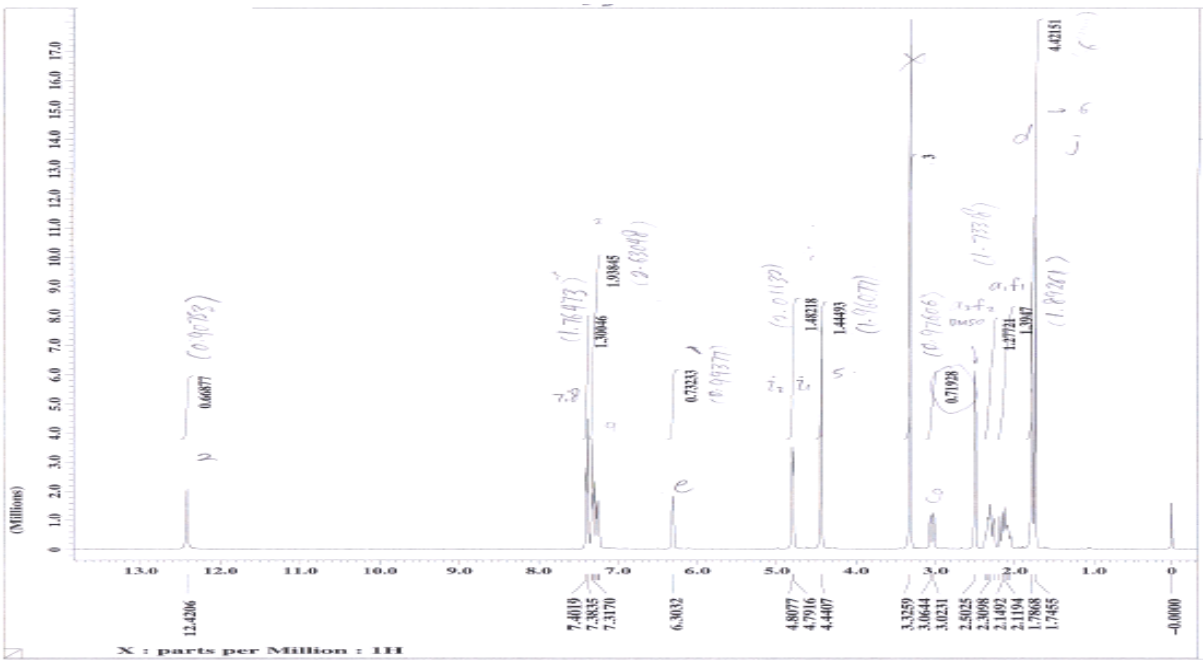

Figure S32: ^{1}H NMR Spectrum for SBRCV

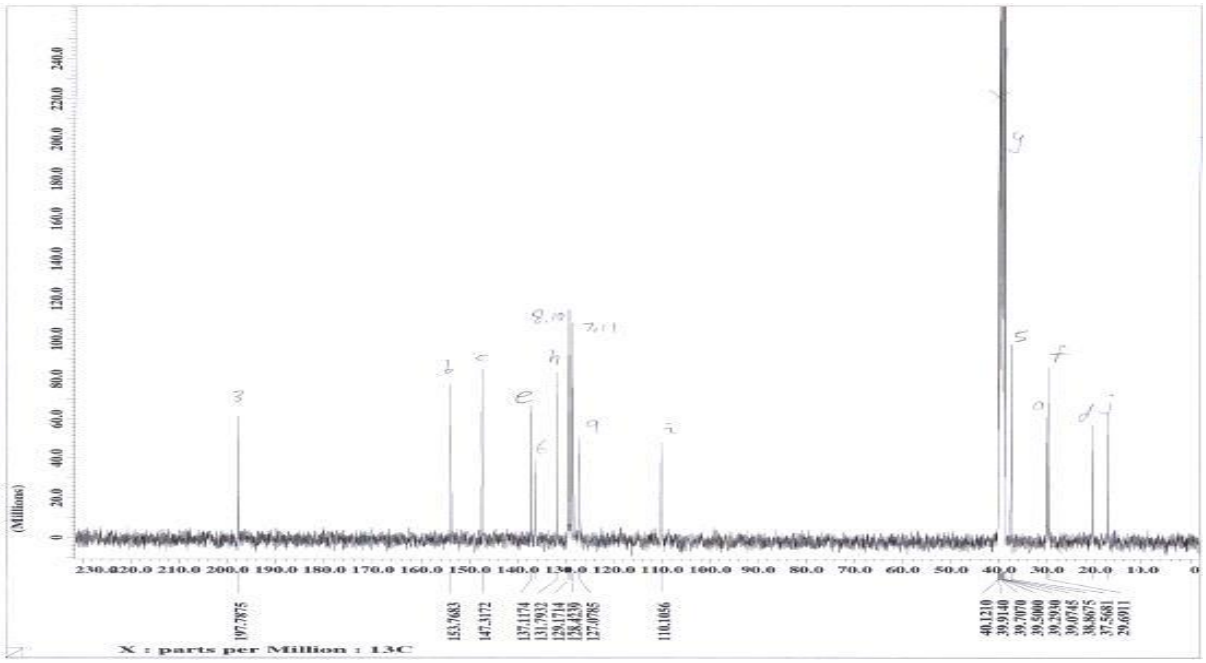

Figure S33: ^{13}C{^{1}H} NMR Spectrum for SBRCV

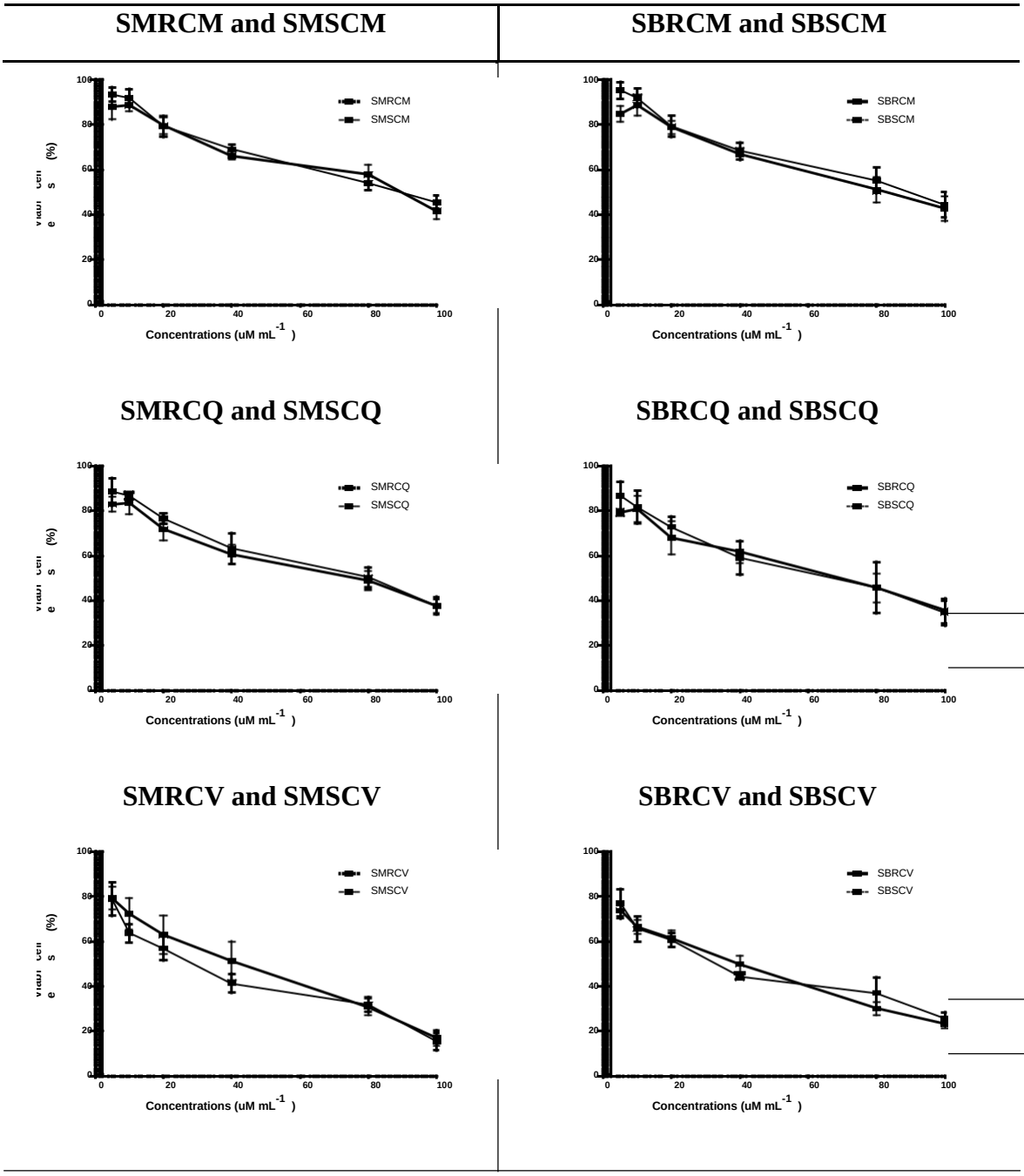

Figure S34: Dose response curves between viable cells (%) against different concentrations of synthetic Schiff bases compounds, calculated through MTT assay against Vero cells. The assays were repeated three times and graph was plotted using Graph Pad Prism Version 5 (Graph Pad Software Inc., San Diego, CA.). The enantiomers were plotted together on same graph to show the similarity of the results between two enantiomers.

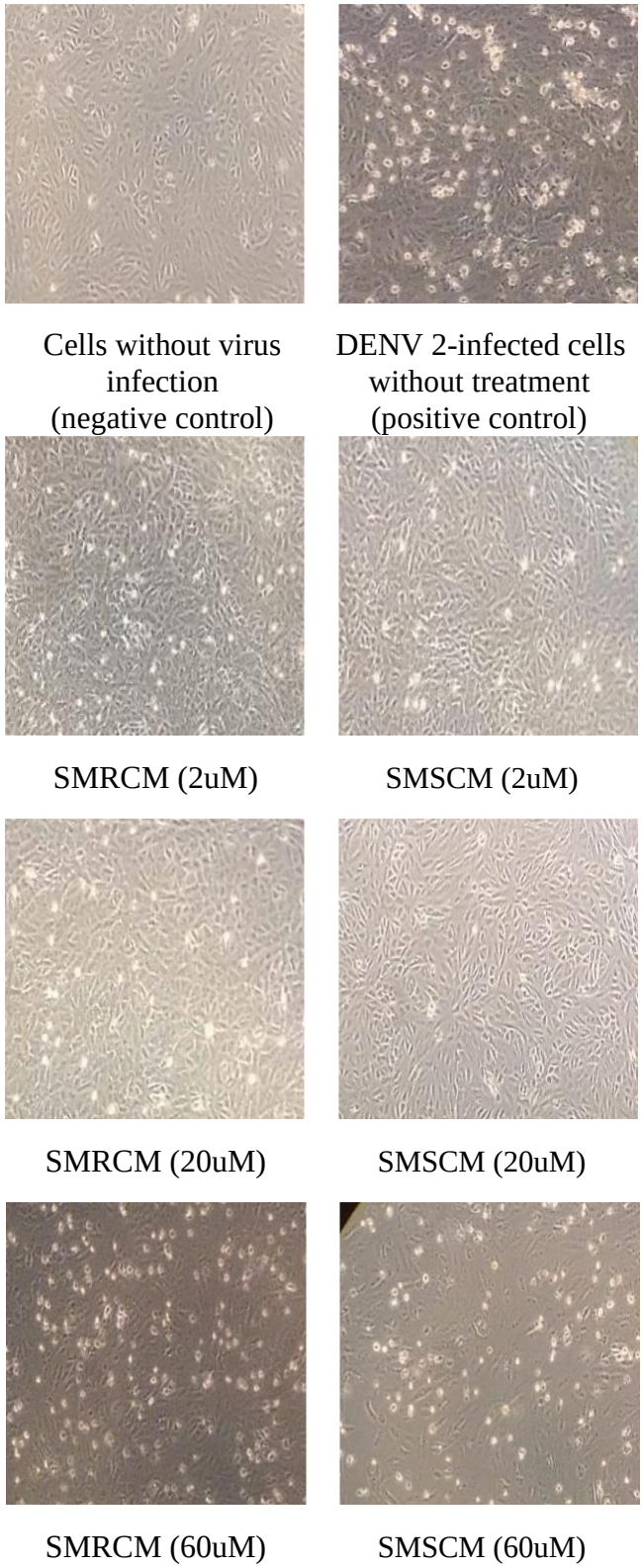

Figure S35a: CPE reduction of DENV 2-infected Vero cells treated with different dilution of compounds SMRCM and SMSCM. The Vero cells monolayers were viewed under inverted microscope at X40 magnification, after four days of incubation. The CPE for each treatment was compared with those of negative and positive controls shown in figure.

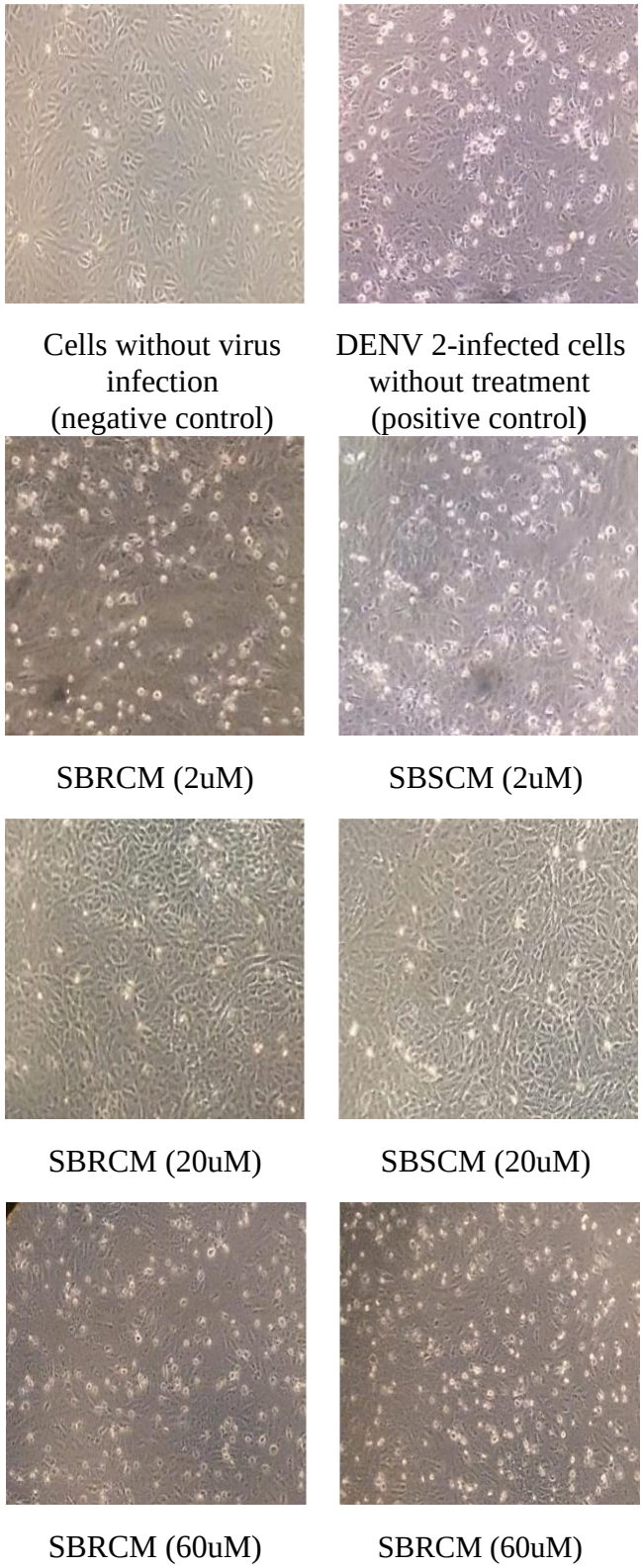

Figure S35b: CPE reduction of DENV 2-infected Vero cells treated with different dilution of compounds SBRCM and SBSCM. The Vero cells monolayers were viewed under inverted microscope at X40 magnification, after four days of incubation. The CPE for each treatment was compared with those of negative and positive controls shown in figure.

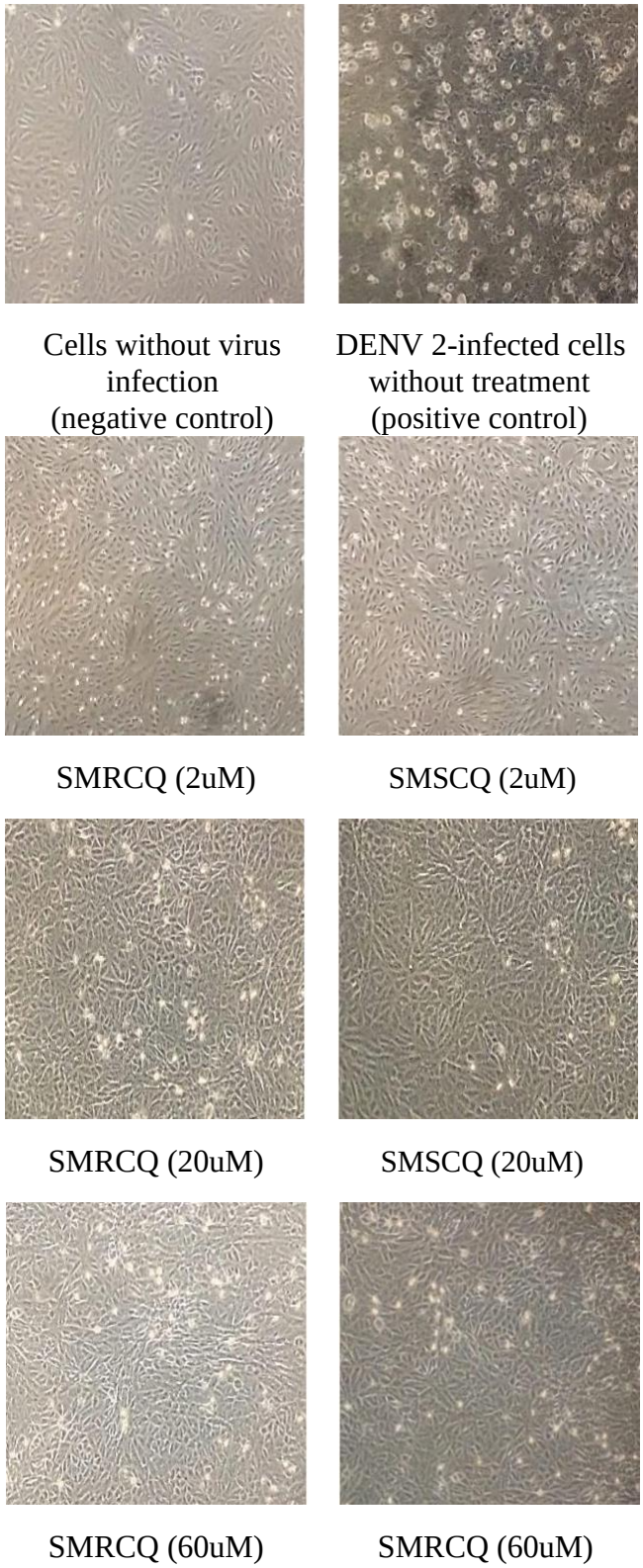

Figure S35c: CPE reduction of DENV 2-infected Vero cells treated with different dilution of compounds SMRCQ and SMSCQ. The Vero cells monolayers were viewed under inverted microscope at X40 magnification, after four days of incubation. The CPE for each treatment was compared with those of negative and positive controls shown in figure.

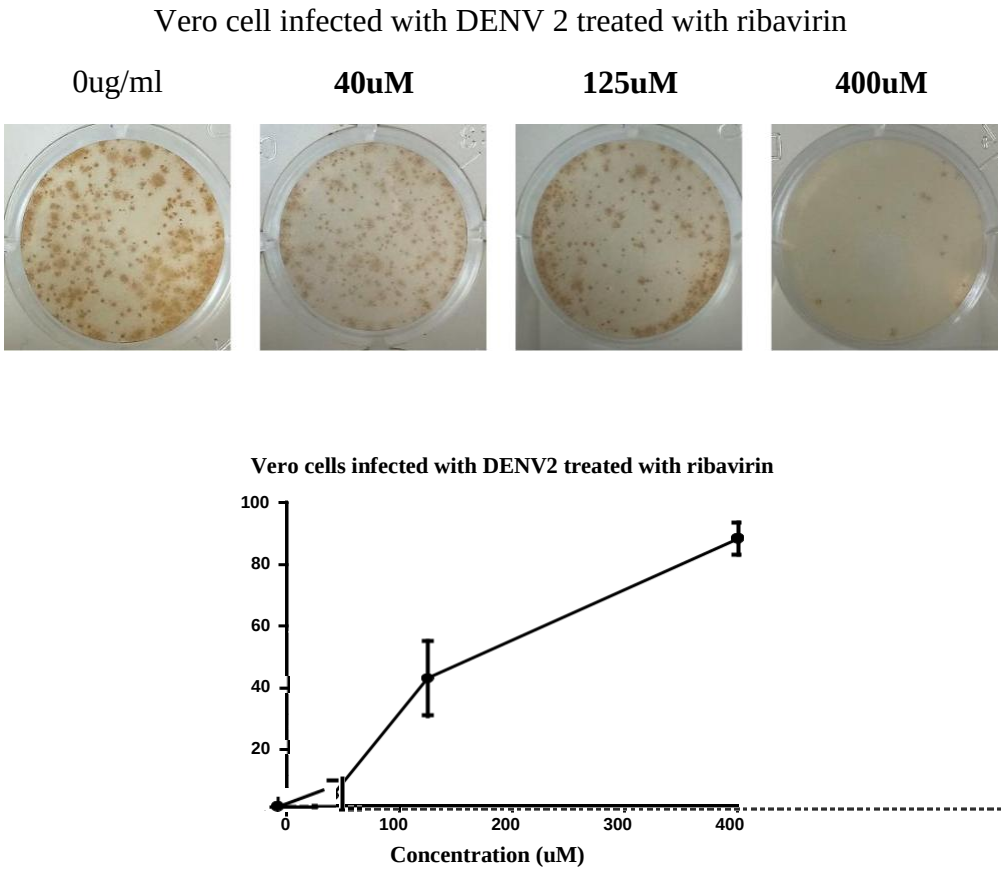

Figure S36: The anti-dengue effects of ribavirin against DENV 2-infected Vero cells. Foci forming unit reduction assay (FFURA) was used to evaluate the *in vitro* antiviral activity of ribavirin against DENV 2 which was behaving in a dose-dependent manner. The percentages of foci reduction were obtained by comparing against untreated cells maintained in parallel. The graph was plotted using Graph Pad Prism Version 5 (Graph Pad Software Inc., San Diego, CA.).

Vero cells infected with DENV 2 treated with SMRCM			
0 uM	1 uM	10 uM	20 uM
			
Vero cells infected with DENV 2 treated with SMSCM			
0 uM	1 uM	10 uM	20 uM
	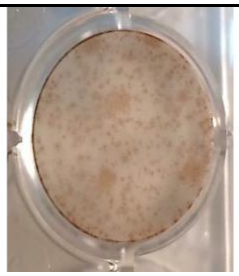		

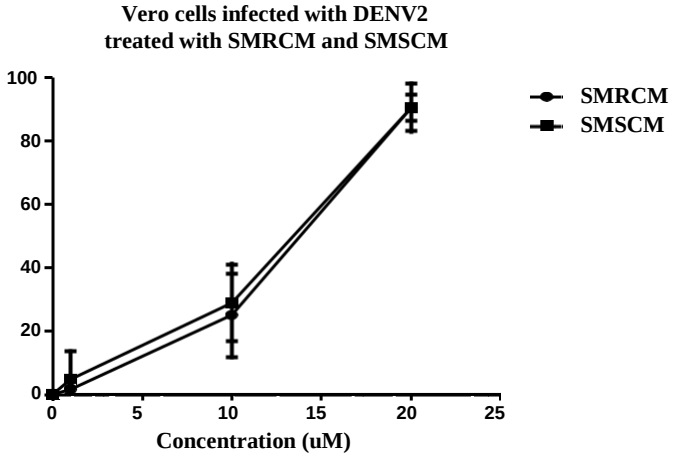

Figure S37a: The anti-dengue effects of SMRCM and SMSCM against DENV 2-infected Vero cells. Foci forming unit reduction assay (FFURA) performed to evaluate anti-dengue activity of SMRCM and SMSCM against DENV 2 which equally inhibited in a dose-dependent manner. The percentages of foci reduction were obtained by comparing against untreated cells maintained in parallel. The dose-response curve was plotted and IC50 dose was calculated using Graph Pad Prism Version 5 (Graph Pad Software Inc., San Diego, CA.).

Vero cells infected with DENV 2 treated with SBRCM			
0 uM	1 uM	10 uM	20 uM
		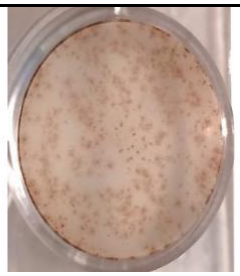	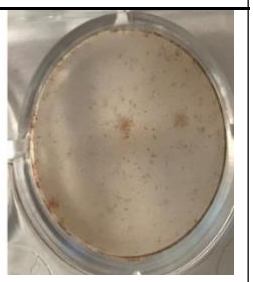
Vero cells infected with DENV 2 treated with SBSCM			
0 uM	1 uM	10 uM	20 uM
	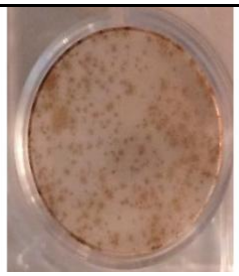	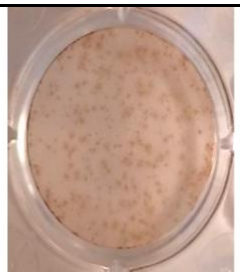	

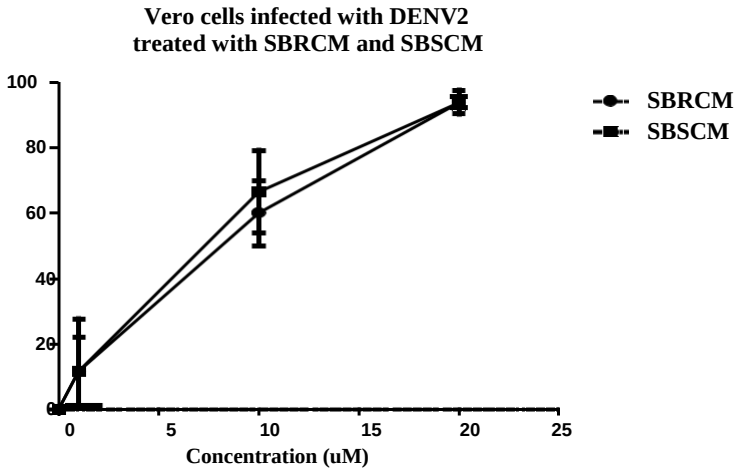

Figure S37b: The anti-dengue effects of SBRCM and SBSCM against DENV 2-infected Vero cells. Foci forming unit reduction assay (FFURA) performed to evaluate anti-dengue activity of SBRCM and SBSCM against DENV 2 which equally inhibited in a dose-dependent manner. The percentages of foci reduction were obtained by comparing against untreated cells maintained in parallel. The dose-response curve was plotted and IC50 dose was calculated using Graph Pad Prism Version 5 (Graph Pad Software Inc., San Diego, CA.).